

Constraining the history of reheating with the NANOGrav 15-year data

Suvashis Maity^{1*}, Nilanjandev Bhaumik^{1,2†}, Md Riajul Haque^{1‡},
Debaprasad Maity^{3¶}, L. Sriramkumar^{1§}

¹Centre for Strings, Gravitation and Cosmology, Department of Physics, Indian Institute of Technology Madras, Chennai 600036, India

²International Centre for Theoretical Physics Asia-Pacific (ICTP-AP), University of Chinese Academy of Sciences, Beijing 100190, China

³Department of Physics, Indian Institute of Technology Guwahati, Guwahati, Assam, India

E-mail: *suvashis@physics.iitm.ac.in, †nilanjandevbhaumik@gmail.com,
‡ria.j.0009@gmail.com, ¶debu@iitg.ac.in, §sriram@physics.iitm.ac.in

Abstract. Over the last few years, primordial black holes (PBHs) have emerged as a strong candidate for cold dark matter. A significant number of PBHs are produced when the strength of the primordial scalar power spectrum is enhanced on small scales (compared to the COBE normalized values on large scales). Such primordial spectra also inevitably lead to strong amplification of the scalar-induced, secondary gravitational waves (GWs) at higher frequencies. The recent detection of the stochastic GW background (SGWB) by the pulsar timing arrays (PTAs) has opened up the possibility of directly probing the very early universe. Different studies have shown that, when PBHs are assumed to have been formed during the epoch of radiation domination, the mechanism for the amplification of the scalar-induced GWs that is required to explain the PTA data can overproduce the PBHs over some ranges of masses. In this work, we assume a specific functional form for the primordial scalar power spectrum and examine the production of PBHs and the scalar-induced secondary GWs during the phase of reheating, which precedes the standard epoch of radiation domination. Specifically, we account for the uncertainties in the conditions for the formation of PBHs and ensure that the extent of PBHs produced remains within the observational bounds. We find that the scalar-induced SGWB generated during a phase of reheating with a steeper equation of state (than that of radiation) fit the NANOGrav 15-year data with a stronger Bayesian evidence than the astrophysical scenario involving GWs produced by merging supermassive binary black holes.

Contents

1	Introduction	1
2	Formation of PBHs during reheating	4
2.1	A brief overview of the dynamics during reheating	4
2.2	Effects of reheating on the formation of PBHs	5
3	Generation of scalar-induced secondary GWs and the PTA data	10
3.1	Spectral density of secondary GWs over wave numbers that re-enter during the phase of reheating	11
3.2	Spectral density of secondary GWs over wave numbers that re-enter during radiation domination	15
3.3	Comparison with the NANOGrav 15-year data	18
3.4	Primary GWs and constraints from ΔN_{eff}	23
4	Conclusions and discussion	25

1 Introduction

During the last few decades, the observations of the cosmic microwave background (CMB) have provided the most effective tool to probe the early universe prior to the surface of the last scattering. The increasingly accurate measurements of the anisotropies in the CMB by COBE [1, 2], WMAP [3–6] and Planck [7–9] have defined the era of precision cosmology. These observations have led to strong constraints on the parameters that characterize the primordial perturbations such as the scalar amplitude A_s , the scalar spectral index n_s , the tensor-to-scalar ratio r , and the scalar non-Gaussianity parameter f_{NL} [10, 11]. However, the CMB constrains the primordial perturbations only on large scales (i.e. wave numbers corresponding to $10^{-4} < k < 1 \text{ Mpc}^{-1}$), and the corresponding bounds on smaller scales are considerably weaker.

Over the past decade, the detection of gravitational waves (GWs) by the Ligo-Virgo-Kagra (LVK) collaboration (in this context, see, for instance, Refs. [12–17]) has led to a paradigm shift in the approach to primordial cosmology. It is now widely recognized that GWs provide a unique window to probe the physics operating in the early universe (see, for example, the recent reviews [18–21]). The GWs observed by the LVK detectors were of astrophysical origin, and they were produced by the mergers of binary black holes (BHs) or neutron stars. As we shall discuss below, there exist a variety of phenomena that can generate GWs in the primordial universe and, importantly, the GWs produced in the early universe will be stochastic in nature. Moreover, because they interact weakly, GWs carry information about the earliest stages of our universe and, hence, they probe primordial physics more effectively than the CMB, in particular, on small scales. But, despite a dedicated effort, the LVK collaboration did not detect a stochastic GW background (SWGGB) over the frequency range of, say, $1 < f < 10^2 \text{ Hz}$, that its detectors are sensitive to [22]. However, a few months ago, this barrier was overcome when the Pulsar Timing Arrays (PTAs)—such as NANOGrav [23, 24], EPTA (including the data from InPTA) [25, 26], PPTA [27, 28], and CPTA [29]—jointly reported the first detection of an SGWB over the frequency range of

$10^{-9} < f < 10^{-6}$ Hz. Specifically, it was found that the SGWB generated by the merging of supermassive BH binaries (SMBHBs) do not statistically explain the observed data in an efficient manner [30]. In fact, the NANOGrav 15-year data favored (with a particularly strong Bayesian evidence) primordial origins for the detected SGWB signal [23, 24, 30]. This has immediately fuelled the search for several different channels for the cosmological generation of the SGWB. These include the SGWB from: (i) models that lead to enhanced formation of primordial BHs (PBHs) [31–40], (ii) domination of ultra-low mass PBHs [41], (iii) mergers due to PBHs [42, 43], (iv) phase transitions in the early universe [44–51], (v) collapse of cosmic strings and domain walls [52–62], (vi) models of axion inflation [36, 63, 64], (vii) blue tilted primary tensor power spectra [65–68], (viii) primordial magnetic fields [69] and (ix) other possible scenarios [70–72].

In this work, we focus on SGWB generated during the formation of PBHs. This is one of the most studied explanations for the PTA data. Nevertheless, we believe that, in the scenario, there are some caveats, such as the overproduction of PBHs, which require further investigation. PBHs are an attractive candidate for dark matter because of their cold, non-interacting nature [73–76]. Contrary to astrophysical BHs, which are typically of the order of solar mass, PBHs can have masses ranging from a few grams to billions of solar masses. PBHs can also play a pivotal role in shaping our understanding of the early universe. While they are constrained in a variety of manner over different mass ranges, there still remains a window over the asteroid mass range where the PBHs can account for the dark matter completely [77]. There are a number of potential mechanisms through which PBHs can form, including bubble collisions [78–80], collapse of domain walls [81–86], collapse of cosmic strings [87–92], electroweak phase transition [93], first-order phase transitions [94, 95], and formation of other topological defects [96, 97]. However, in this work, we shall be interested in the scenario wherein PBHs are formed due to the collapse of the enhanced density perturbations that originated during inflation [98–108].

Inflation corresponds to the earliest phase of accelerated expansion of our universe. Though it was initially proposed to resolve the horizon problem, the success of inflation lies in the fact that it also provides a mechanism for the creation of the primordial scalar and tensor perturbations (in this regard, see the reviews [109–115]). While the inflationary scalar perturbations contribute to the density fluctuations and result in the emergence of structure in the universe, the tensor perturbations correspond to GWs. These perturbations are eventually responsible for the anisotropies observed in the CMB and the distribution of the large-scale structure that we see around us today. The observations of the anisotropies in the CMB by missions such as Planck [10, 116] and BICEP/Keck [117] allow us to strongly constrain the primordial scalar power spectrum around the pivot scale of $k_* = 0.05 \text{ Mpc}^{-1}$. But, as we mentioned, the constraints on the primordial scalar power spectrum are considerably weaker over smaller scales, say, corresponding to wave numbers $k \gg 10^5 \text{ Mpc}^{-1}$. Due to this reason, the scalar power spectrum can, in principle, be considerably amplified on small scales (when compared to the COBE normalized values on large scales), leading to the formation of a significant number of PBHs when the concerned wave numbers re-enter the Hubble radius after inflation. Such power spectra with enhanced power on small scales can be generated during inflation with the aid of potentials that contain either a point of inflection [100, 103, 105, 118–123] or a small bump/dip [124]. They can also be generated in inflationary models involving more than one field [125–129], due to resonant amplification during inflation [130, 131] or from squeezed initial states [132]. At the first order in perturbation theory, the scalar and tensor perturbations are decoupled and hence evolve independently. However, at the higher

order in the perturbations, one form of perturbation can act as a source for the other. As a result, when the amplitude of the scalar perturbations at the first order is enhanced over small scales to produce a significant number of PBHs, they inevitably induce tensor perturbations of considerable strengths at the second order. In such scenarios, the PBHs form almost instantaneously when the wave numbers with significant scalar power re-enter the Hubble radius and, in the process, also generate a SGWB of amplitudes that are comparable to the sensitivities of the ongoing and forthcoming GW observatories.

The formation of PBHs and the generation of scalar-induced, secondary GWs during the epoch of radiation domination have been discussed in the literature in good detail, particularly in the context of the PTA data. The main caveat in this scenario remains the fine-tuning and the possible overproduction of PBHs in a certain range of masses [31]. This issue has motivated further studies wherein the formation of PBHs has been considered during non-standard histories post inflation [40, 133–137]. Reheating is the phase that immediately follows inflation. During this period, the inflaton oscillates at the bottom of the inflationary potential, and, with the aid of suitable couplings, the energy from the inflaton is transferred to the fields that constitute the standard model of particle physics. In principle, the PBHs can form during the phase of reheating and, in such a scenario, the parameters such as the effective equation-of-state (EoS) during reheating and the reheating temperature will affect the formation mechanism as well as the number of PBHs produced [138]. An epoch of reheating with a general EoS can also significantly alter the strength and the spectral shape of the secondary GWs [20, 139, 140]. In this study, we focus on the formation of PBHs during the phase of reheating and explore the manner in which such a scenario can explain the observed PTA data. We take into account the uncertainties in the conditions for the collapse of the PBHs as well as the existing bounds on the abundance of PBHs in the relevant range of masses. We assume an analytical expression for the inflationary scalar power spectrum, which is in the form of a broken power law. Such a spectral shape is motivated by the forms of the scalar power spectra that typically arise when one considers models of inflation that permit a brief epoch of ultra slow roll [123, 141]. We scan our parameter space for an optimal fit to the NANOGrav 15-year data, while staying strictly within the observational bounds on the abundance of the PBHs. We perform a Bayesian analysis and compare our scenario with the possible astrophysical explanation for the PTA results through the mergers of SMBHBs. We find that, when we allow room for uncertainties in the conditions for the collapse of PBHs, our model is strongly preferred over the scenario involving SMBHBs.

This paper is organized as follows. In Sec. 2, we shall briefly describe the dynamics of the epoch of reheating and the formation of PBHs during the epoch. In particular, we shall discuss the effects of the parameters describing the epoch of reheating on the abundance of PBHs and the fraction of cold dark matter that can be constituted of PBHs. In Sec. 3 we shall study the associated generation of secondary GWs (due to the enhanced scalar power on small scales) and its prospects in explaining the observations by the PTAs. We shall carry out a complete Bayesian analysis when comparing the models with the NANOGrav 15-year data. We shall further discuss the implications of our results on the energy scale of inflation or, equivalently, on the tensor-to-scalar ratio in the context of primary GWs. In Sec. 4, we shall summarize our results and conclude with a discussion on their implications.

At this stage of our discussion, let us make a few clarifying remarks on the conventions and notations that we shall adopt in this work. We shall work with natural units such that $\hbar = c = 1$, and set the reduced Planck mass to be $M_{\text{Pl}} = (8\pi G)^{-1/2} \simeq 2.4 \times 10^{18}$ GeV. We shall adopt the signature of the metric to be $(-, +, +, +)$. Note that Latin indices shall

represent the spatial coordinates, except for k which shall be reserved for denoting the wave number. We shall assume the background to be spatially flat Friedmann-Lemaître-Robertson-Walker (FLRW) line element described by the scale factor a and the Hubble parameter H . Also, an overdot and an overprime shall denote differentiation with respect to the cosmic time t and the conformal time η , respectively.

2 Formation of PBHs during reheating

In this section, after a brief overview of the dynamics of reheating, we shall describe the formation of PBHs during the epoch. We shall also compare the extent of PBHs formed with the constraints on the quantity $f_{\text{PBH}}(M)$, which denotes the fraction of PBHs that contribute to the energy density of cold dark matter.

2.1 A brief overview of the dynamics during reheating

The phase of reheating connects the epochs of inflation and radiation domination. Consider the simplest scenario of inflation driven by a single, canonical, scalar field, say, ϕ , governed by the potential $V(\phi)$. In such a case, after the end of inflation, the inflaton oscillates about a minima of the potential. The inflaton is assumed to be coupled (either directly or indirectly) to the fields that constitute the standard model of particle physics. As the inflaton oscillates, it is expected to eventually decay into the particles that constitute the standard model and thermalize, thereby leading to the epoch of radiation domination and setting appropriate initial conditions for big bang nucleosynthesis (BBN) to be realized. Over the years, several reheating mechanisms have been proposed based on either non-perturbative [142–146] or perturbative processes with non-gravitational and gravitational interactions [147–151]. In this work, we shall consider the simple perturbative reheating scenario with a constant decay width, say, Γ_ϕ , for the inflaton. Depending upon the decay width, the process of reheating can be either instantaneous with the maximum temperature of $T_{\text{re}} \simeq 10^{15}$ GeV or it may be prolonged with the minimum possible temperature of $T_{\text{re}} = T_{\text{BBN}} \simeq 4$ MeV [152, 153]. The duration of the phase of reheating depends on the decay width Γ_ϕ and the behavior of the potential $V(\phi)$ near a minima.

With the introduction of the coupling to the other fields through the decay width Γ_ϕ , the equation of motion describing the inflaton is modified to be (in this context, see, for instance, Ref. [114])

$$\ddot{\phi} + (3H + \Gamma_\phi)\dot{\phi} + V_\phi(\phi) = 0, \quad (2.1)$$

where, as we mentioned, H is the Hubble parameter and $V_\phi = dV/d\phi$. As the inflaton oscillates about a minima of the potential, we can define an effective EoS parameter to describe the phase of reheating as $w_\phi = \langle p_\phi \rangle / \langle \rho_\phi \rangle$, where ρ_ϕ and p_ϕ denote the energy density and pressure associated with the inflaton and the angular brackets represent the time average over an oscillation. If we assume that the potential has the form $V(\phi) \propto \phi^n$ near the minimum, upon averaging over a single oscillation, we obtain that [154]

$$w_\phi = \frac{n-2}{n+2}. \quad (2.2)$$

Note that, for $n = 2$, i.e. when the potential behaves quadratically near the minimum, we have $w_\phi = 0$, which indicates that reheating behaves as a matter-dominated phase. Similarly, when $n = 4$, i.e. in the quartic case, we have $w_\phi = 1/3$, which corresponds to the EoS during

a radiation-dominated epoch. In principle, w_ϕ can be as high as unity, which corresponds to a phase of kination, i.e. when the kinetic energy of the scalar field completely dominates the potential energy. In the scenario of perturbative reheating of our interest, the equation of motion (2.1) for ϕ can be obtained from the following equation that governs the energy density ρ_ϕ of the scalar field:

$$\dot{\rho}_\phi + 3H(1 + w_\phi)\rho_\phi = -\Gamma_\phi(1 + w_\phi)\rho_\phi. \quad (2.3)$$

The conservation of the total energy of the system involving the scalar field and radiation then leads to the following equation for the energy density of radiation ρ_R :

$$\dot{\rho}_R + 4H\rho_R = \Gamma_\phi(1 + w_\phi)\rho_\phi. \quad (2.4)$$

Due to the transfer of energy from the inflaton, the dimensionless energy density of radiation, viz. $\rho_R/(\rho_R + \rho_\phi)$, keeps growing until it approaches unity, marking the end of reheating at a given conformal time, say, η_{re} . It is often found that, throughout the entire period, except towards the end, the reheating phase is governed by the inflaton EoS w_ϕ . Hence, we shall assume that the EoS is constant throughout the reheating phase at a given value $w_{\text{re}} = w_\phi$. This allows us to describe the reheating phase in terms of only two parameters: the EoS parameter during reheating w_{re} and the reheating temperature T_{re} , which is the temperature of the radiation when reheating is complete.

During the phase of reheating with a general EoS parameter w_{re} , upon using the first Friedmann equation and the equation governing the conservation of energy, we can arrive at the following expressions for the scale factor and the Hubble parameter:

$$a(\eta) \propto \eta^{2/(1+3w_{\text{re}})}, \quad H(\eta) \propto \eta^{-3(1+w_{\text{re}})/(1+3w_{\text{re}})}. \quad (2.5)$$

On matching the scale factor and the Hubble parameter at η_{re} , i.e. at the conformal time at the end of reheating, we can arrive at the corresponding expressions for the scale factor a and the Hubble parameter H during the epoch of radiation domination to be

$$a(\eta) \propto \eta - \left(\frac{1-3w_{\text{re}}}{2}\right)\eta_{\text{re}}, \quad H(\eta) \propto \left[\eta - \left(\frac{1-3w_{\text{re}}}{2}\right)\eta_{\text{re}}\right]^{-2}. \quad (2.6)$$

Let $k_{\text{re}} = a(\eta_{\text{re}})H(\eta_{\text{re}})$ and $k_{\text{eq}} = a(\eta_{\text{eq}})H(\eta_{\text{eq}})$ be the wave numbers that re-enter the Hubble radius at the end of reheating and at radiation-matter equality (corresponding to conformal time η_{eq}), respectively. Using the conservation of entropy, we can relate k_{re} to k_{eq} as follows:

$$\frac{k_{\text{eq}}}{k_{\text{re}}} = \frac{a_{\text{re}}}{a_{\text{eq}}} = \left(\frac{g_{\text{s,eq}}}{g_{\text{s,re}}}\right)^{1/3} \frac{T_{\text{eq}}}{T_{\text{re}}}, \quad (2.7)$$

where, it can be shown that, $a_{\text{eq}}^{-1} = 24000 \Omega_{\text{m}} h^2$, $k_{\text{eq}} = 0.07 \Omega_{\text{m}} h^2 \text{Mpc}^{-1}$ and the temperature at equality being $T_{\text{eq}} = 5.6 (\Omega_{\text{m}} h^2) \text{eV}$. Note that we have expressed all the expressions in terms of the present day matter density parameter $\Omega_{\text{m}} h^2 = 0.13$ [155].

2.2 Effects of reheating on the formation of PBHs

In this section, we shall discuss the formation of PBHs due to the enhancement in power on small scales in the spectrum of curvature perturbations generated during inflation. In the simple picture wherein reheating occurs instantaneously after inflation, all the small-scale

modes re-enter the Hubble radius during the epoch of radiation domination. When scalar perturbations with significant amplitudes re-enter the Hubble radius, the overdense region collapses almost instantaneously to form PBHs. The mass of the PBHs thus produced turns out to be nearly equivalent to the mass within the Hubble radius at the time of re-entry. When there occurs a phase of reheating, some of the small-scale modes re-enter the Hubble radius during reheating. Even in such a situation, as the reheating dynamics can be described by an effective EoS, the mechanism for the formation of the PBHs proves to be the same. However, apart from the amplitude of the scalar power spectrum, the efficiency of the formation of PBHs during reheating depends on the EoS. We shall focus on the collapse of the overdense regions due to the large scalar perturbations generated during inflation, which ensures instantaneous collapse. We should mention that the location of the peak in the inflationary scalar power spectrum determines the time of re-entry of that scale, and thus the time of PBH formation. Late-forming PBHs correspond to peaks at smaller wave numbers and thus lead to PBHs of higher masses. PBHs with mass $M < 10^{15}$ g would have evaporated by today due to Hawking radiation. In this work, we shall be interested in PBHs with mass $M > 10^{15}$ g, which can contribute to the cold dark matter.

In our analysis, we shall not consider any specific inflationary potential for generating the scalar power spectrum. Rather, we shall consider an analytical scalar power spectrum with a broken power law form. On large scales, we shall assume that the power spectrum is nearly scale invariant, as is required to fit the CMB data. On small scales, we shall assume that the power spectrum rises as k^4 as it approaches the peak and, beyond the peak, it falls as k^{n_0} with $n_0 < 0$. We should point out that such power spectra arise in single-field models of inflation that permit a brief period of ultra slow roll [141]. The complete form of the scalar power spectrum that we shall work with is given by

$$\mathcal{P}_{\mathcal{R}}(k) = A_{\text{s}} \left(\frac{k}{k_*} \right)^{n_{\text{s}}-1} + A_0 \begin{cases} \left(\frac{k}{k_{\text{peak}}} \right)^4 & k \leq k_{\text{peak}}, \\ \left(\frac{k}{k_{\text{peak}}} \right)^{n_0} & k \geq k_{\text{peak}}, \end{cases} \quad (2.8)$$

where A_{s} and n_{s} are the amplitude and spectral index of the power spectrum at the CMB pivot scale of $k_* = 0.05 \text{ Mpc}^{-1}$. Note that k_{peak} denotes the wave number at which the peak is located and A_0 represents the extent of enhancement of the power spectrum at the location of the peak when compared to the nearly scale-invariant amplitude on large scales. Later, when we calculate the extent of PBHs produced and the strengths of the secondary GWs generated, we shall assume the values of A_{s} and n_{s} to be as suggested by the recent Planck data [10].

To calculate the abundance of PBHs, the two most popular methods that are often used in the literature are the Press-Schechter formalism [156] and peak theory [157]. In general, the results from these two established methods for calculating the probability of collapse to form PBHs do not converge, even when all the other conditions and parameters are fixed (in this context, see Refs. [122, 158–160]). Also, there have been recent efforts from different groups to understand the efficiency of collapse leading to the formation of PBHs with the aid of more involved and accurate numerical frameworks using the so-called compaction function methods (see, for example, Refs. [161–167]). These efforts indicate that small differences in the details of implementation lead to rather different final results. In this work, we shall follow the simple Press-Schechter formalism which considers a Gaussian random field for the initial density fluctuations and a constant critical density contrast for the formation of PBHs.

Let $P(\delta)$ denote the probability distribution of the density contrast δ , and let δ_c denote the critical value of the density contrast above which the overdense regions collapse to form PBHs. The fraction of the density that collapses to form PBHs (often referred to as the PBH mass fraction), i.e. $\beta(M) = \rho_{\text{PBH}}/\rho_{\text{total}}$, is then given by

$$\beta(M) = \int_{\delta_c}^{\infty} d\delta P(\delta) \simeq \frac{1}{2} \operatorname{erfc} \left\{ \frac{\delta_c}{\sqrt{2} \sigma_\delta(M)} \right\}, \quad (2.9)$$

where, in arriving at the final expression, we have assumed that the probability distribution $P(\delta)$ is a Gaussian function. During the phase of reheating or the epoch of radiation domination, the power spectrum, say, $\mathcal{P}_\delta(k)$, associated with the density contrast is related to the primordial power spectrum of the curvature perturbation $\mathcal{P}_\mathcal{R}(k)$ through the relation [168]

$$\mathcal{P}_\delta(k) = \left[\frac{2(1+w_{\text{re}})}{5+3w_{\text{re}}} \right]^2 \left(\frac{k}{aH} \right)^4 \mathcal{P}_\mathcal{R}(k). \quad (2.10)$$

If $\sigma_\delta(R)$ represents the variance in the density fluctuations in space, which is arrived at by smoothing over a radius R with the help of the window function $W(kR)$, then the quantity is given in terms of the power spectrum $\mathcal{P}_\delta(k)$ through the relation

$$\sigma_\delta^2(R) = \int d \ln k \mathcal{P}_\delta(k) W^2(kR). \quad (2.11)$$

As is often done, we shall assume the window function to be of the following Gaussian form: $W(kR) = \exp(-k^2 R^2/2)$. We are yet to relate the radius R and the mass M that the variance σ_δ depends on. We shall discuss this point below.

Let M_{H} be the total mass within the Hubble radius H^{-1} at a given time, and let M_{eq} be the mass within the Hubble radius at the time of radiation-matter equality. The mass M of the PBHs formed due to collapse is related to the quantity M_{H} at the time of formation as follows [169]:

$$M \equiv \gamma M_{\text{H}} = \gamma \frac{4\pi \rho_{\text{total}}}{3H^3} \Big|_{k=aH}, \quad (2.12)$$

where ρ_{total} denotes the total energy density of the background and γ is the efficiency of collapse given by $\gamma = w_{\text{re}}^{3/2}$ ¹. For a given reheating temperature T_{re} , we can relate the mass M of the PBHs at the time of their formation to the quantity M_{eq} as

$$\frac{M}{M_{\text{eq}}} = \gamma \left(\frac{g_{\text{eq}}}{g_{\text{re}}} \right)^{1/2} \left[\left(\frac{43}{11 g_{\text{s, re}}} \right)^{1/3} \sqrt{\frac{\pi^2 g_{\text{re}}}{90}} \frac{T_0}{k} \right]^{\frac{3(1+w_{\text{re}})}{1+3w_{\text{re}}}} \left(\frac{T_{\text{eq}}}{M_{\text{Pl}}} \right)^2 \left(\frac{T_{\text{re}}}{M_{\text{Pl}}} \right)^{\frac{1-3w_{\text{re}}}{1+3w_{\text{re}}}}, \quad (2.14)$$

¹At this point, we should mention that there exists a more accurate method to estimate the mass M of the PBHs, with the mass being sensitive to the EoS parameter, say, w_{re} , of the cosmological background fluid as well as the profile of the scalar fluctuations [170–177]. In the study of critical phenomena in gravitational collapse, numerical simulations have demonstrated that the mass of PBHs obey a scaling relation when the amplitude of the perturbation is close to the critical value (i.e. when $\delta_{\text{m}} - \delta_c \leq 10^{-2}$, where δ_{m} is the initial amplitude of the perturbation). According to the scaling relation, the mass of the PBHs is given by

$$M = \kappa M_{\text{H}} (\delta_{\text{m}} - \delta_c)^{\gamma_{\text{f}}}, \quad (2.13)$$

where the exponent γ_{f} depends on the EoS parameter w_{re} , while the overall constant κ and the critical density δ_c depend both on w_{re} and the shape of the scalar power spectrum (in this context, see Refs. [170, 174, 178]; for a discussion on the dependence of γ_{f} on w_{re} , see Ref. [179], Tab. 1 and Ref. [180], Fig. 7). However, we find that analytical estimates of γ_{f} and κ , which would have been helpful, are yet to be arrived at in the literature.

where g_{re} and g_{eq} are the effective relativistic degrees of freedom that contribute to the energy density of radiation at the times of reheating and equality, respectively, and $g_{\text{s, re}}$ represents the number of relativistic degrees of freedom that contribute to the entropy of radiation at the end of reheating. Moreover, T_0 represents the temperature of the CMB today. We now need to relate the wave number k that appears in the above expression for M to the radius R over which the variance σ_δ is smoothed over. In the absence of any other scale in the problem, we shall assume that $k = R^{-1}$, which then allows us to relate the radius R to the mass M of the PBHs.

The quantity $\beta(M)$ is exponentially sensitive to δ_c and there is a significant amount of uncertainty in choosing a suitable value for δ_c (in this regard, see, for instance, Ref. [122], App. B). The critical value of the density contrast δ_c should depend on the shape of the curvature power spectrum [162, 181]. Also, even for a Gaussian distribution of scalar perturbations, the non-linear relationship between the density contrast and the curvature perturbation leads to a non-Gaussian distribution for the density contrast [182, 183]. Moreover, during inflation, the mechanism that produces the scalar power spectrum with sharp features can also generate large levels of non-Gaussianities [123, 132, 184]. Further, many models of PBH formation predict a non-Gaussian tail for the primordial distribution of the curvature perturbation (in this context, see, for example, Refs. [185, 186]). Since, in this work, we do not consider any particular model of inflation, we shall leave a more accurate estimation of the combined effects of non-Gaussianities, arising during inflation and due to the non-linearities post-inflation, for future work. We shall assume that the threshold value of the density contrast is given by the following analytical expression [187]:

$$\delta_c^{\text{an}} = \frac{3(1+w_{\text{re}})}{5+3w_{\text{re}}} \sin^2 \left(\frac{\pi \sqrt{w_{\text{re}}}}{1+3w_{\text{re}}} \right). \quad (2.15)$$

It is important to recognize that different models for the collapse of PBHs lead to different values of δ_c . In what follows, we shall utilize the above analytical estimate for δ_c to investigate the dependence of the number of PBHs formed on the reheating parameters. In due course, we shall also discuss the effects of the variation of δ_c .

Let $f_{\text{PBH}}(M)$ denote the present-day, fractional contribution of PBHs to the density of cold dark matter, i.e. $f_{\text{PBH}} = \Omega_{\text{PBH}}/\Omega_c$. Note that the energy density of PBHs ρ_{PBH} always varies as a^{-3} whereas, during reheating, the energy density of the background behaves as $\rho_{\text{total}} \propto a^{-3(1+w_{\text{re}})}$. Therefore, during reheating, $\rho_{\text{PBH}}/\rho_{\text{total}} \propto a^{3w_{\text{re}}}$. In contrast, during the epoch of radiation domination which follows reheating, since total energy density varies as a^{-4} , we find that $\rho_{\text{PBH}}/\rho_{\text{total}} \propto a$. Thus, one can express $f_{\text{PBH}}(M)$ corresponding to mode k as

$$f_{\text{PBH}}(k) = \frac{\beta(k)}{0.42} \left(\frac{k}{k_{\text{re}}} \right)^{\frac{6w_{\text{re}}}{1+3w_{\text{re}}}} \left(\frac{a_{\text{eq}}}{a_{\text{re}}} \right) = \frac{\beta(M)}{0.42} \left(\frac{k}{k_{\text{re}}} \right)^{\frac{6w_{\text{re}}}{1+3w_{\text{re}}}} \left(\frac{g_{\text{s, re}}}{g_{\text{s, eq}}} \right)^{1/3} \frac{T_{\text{re}}}{T_{\text{eq}}}, \quad (2.16)$$

where we have set $\Omega_c^{\text{eq}} = 0.42$. From Eqs. (2.14) and (2.16), we can see that both the mass of PBHs and their abundance depend on T_{re} and w_{re} . After some algebra, it can be shown that the quantity $f_{\text{PBH}}(M)$ can be expressed as follows:

$$f_{\text{PBH}}(M) = \beta(M) \frac{\Omega_{\text{m}} h^2}{\Omega_c h^2} \left(\frac{g_{\text{s, eq}}}{g_{\text{s, re}}} \right) \left(\frac{g_{\text{re}}}{g_{\text{eq}}} \right)^{\frac{1}{1+w_{\text{re}}}} \left(\frac{T_{\text{re}}}{T_{\text{eq}}} \right)^{\frac{1-3w_{\text{re}}}{1+w_{\text{re}}}} \left(\frac{M}{\gamma M_{\text{eq}}} \right)^{-\frac{2w_{\text{re}}}{1+w_{\text{re}}}}. \quad (2.17)$$

In Fig. 1, assuming specific values of the parameters A_0 and n_0 that describe the inflationary scalar power spectrum, we have illustrated the behavior of $f_{\text{PBH}}(M)$ for a range

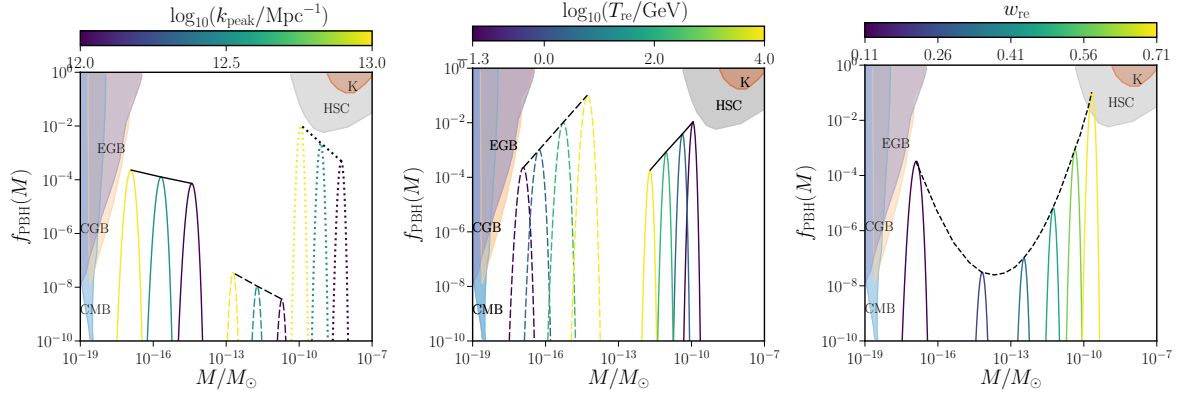


Figure 1. The quantity f_{PBH} is plotted as a function of M/M_{\odot} for a range of k_{peak} , T_{re} and w_{re} (in the left, middle and right panels). We have set $A_0 = 10^{-1.5}$ and $n_0 = -2$ in plotting these figures. In the left panel, we have fixed $T_{\text{re}} = 50$ MeV and have plotted $f_{\text{PBH}}(M)$ for three different values of k_{peak} and for three different values of w_{re} , viz. $w_{\text{re}} = (1/9, 1/3, 2/3)$ (as solid, dashed and dotted lines). We should mention that the peak values of $f_{\text{PBH}}(M)$ behaves as $M^{-2w_{\text{re}}/(1+w_{\text{re}})}$ and, in particular, as $M^{-1/2}$ when $w_{\text{re}} = 1/3$ [188]. In the middle panel, we have fixed k_{peak} at 10^{13} Mpc^{-1} and have plotted $f_{\text{PBH}}(M)$ for four different values of T_{re} and for the two different values of $w_{\text{re}} = (1/9, 2/3)$ (as solid and dashed lines). The slopes of the peaks of $f_{\text{PBH}}(M)$ in this case behave approximately as ± 1 . In the right panel, we have set $T_{\text{re}} = 50$ MeV and $k_{\text{peak}} = 10^{13} \text{ Mpc}^{-1}$ and have plotted $f_{\text{PBH}}(M)$ for the six different values of w_{re} in the range $0.1 < w_{\text{re}} < 0.7$. We see that $f_{\text{PBH}}(M)$ has the lowest value when $w_{\text{re}} = 1/3$ and it keeps increasing for values away from it.

of values of the parameters k_{peak} , T_{re} and w_{re} . In the left panel of the figure, assuming $T_{\text{re}} = 50$ MeV, we have plotted the quantity $f_{\text{PBH}}(M)$ for values of k_{peak} that lie in the range $10^{12} < k_{\text{peak}} < 10^{13} \text{ Mpc}^{-1}$. In the panel, we have also plotted the quantity for three values of w_{re} , viz. $w_{\text{re}} = (1/9, 1/3, 2/3)$. We find that the corresponding slopes of the peaks of $f_{\text{PBH}}(M)$ behave as $-1/5$, $-1/2$, and $-4/5$, as suggested by Eq. (2.17). In the middle panel, assuming $k_{\text{peak}} = 10^{12} \text{ Mpc}^{-1}$, we have illustrated the behavior of $f_{\text{PBH}}(M)$ for different values of T_{re} , with w_{re} set to $1/9$ and $2/3$. On combining Eqs. (2.14) and (2.17), we can see that, as T_{re} is changed, for $w_{\text{re}} < 1/3$, $f_{\text{PBH}}(M)$ behaves as M , whereas, for $w_{\text{re}} > 1/3$, it varies as M^{-1} , a point which is also evident from the middle panel. (Though, we should clarify that there is a slight deviation from such behavior due to the temperature-dependent coefficients g_{re} and $g_{\text{s, re}}$.) In the right panel of the figure, assuming $k_{\text{peak}} = 10^{13} \text{ Mpc}^{-1}$ and $T_{\text{re}} = 50$ MeV, we have plotted $f_{\text{PBH}}(M)$ for six different values of w_{re} , ranging from 0.1 to 0.7 . It is clear that the maximum value of $f_{\text{PBH}}(M)$ is the lowest when $w_{\text{re}} = 1/3$ and it increases as we move away from $w_{\text{re}} = 1/3$. In the figure, apart from $f_{\text{PBH}}(M)$ we have calculated, we have indicated the current observational constraints on the quantity. The constraints that we have included are from the extragalactic gamma-ray background (EGB) [189, 190], from the CMB [191, 192], and from the microlensing searches by Subaru (HSC) [193, 194] as well as Kepler (K) [195]. We should clarify that these constraints have been arrived at assuming a monochromatic distribution of the PBH mass and they need to be modified for extended mass functions.

It is evident from our analysis that the mass M of the PBHs and the quantity $f_{\text{PBH}}(M)$ not only depend on the inflationary scalar power spectrum but also on the parameters describing the epoch of reheating. However, certain behavior, such as $f_{\text{PBH}}(M) \propto T_{\text{re}}^{\frac{1-3w_{\text{re}}}{1+w_{\text{re}}}} M^{-\frac{2w_{\text{re}}}{1+w_{\text{re}}}}$

remains valid irrespective of the shape of the power spectrum, whereas the actual value of the PBH mass fraction naturally depends on all the parameters involved. We should also point out that, for the power spectrum (2.8) we have considered, the $f_{\text{PBH}}(M)$ proves to be nearly monochromatic in nature.

There is another point that we need to clarify at this stage of our discussion. Note that the pre-factor $(1 + w_{\text{re}})/(5 + 3w_{\text{re}})$ in $\mathcal{P}_\delta(k)$ and δ_c^{an} [see Eqs. (2.10) and (2.15)], which originates from the Poisson equation, cancel each other on substituting them in the expression (2.9) for $\beta(M)$. We find that the term $\sin^2[\pi \sqrt{w_{\text{re}}}/(1 + 3w_{\text{re}})]$ that appears in the expression (2.15) for δ_c^{an} has a global maximum at $w_{\text{re}} = 1/3$. Since the maximum of δ_c^{an} occurs at $w_{\text{re}} = 1/3$, the abundance of PBHs has a minimum at the value. It is due to this reason that, at the time of radiation-matter equality, the quantity $f_{\text{PBH}}(M)$ exhibits a similar dependence on w_{re} , as we have shown in the right panel of Fig. 1. However, we should add that such a dependence of $\beta(M)$ on w_{re} follows from the formalism we have adopted to estimate the number of PBHs formed [187]. Such a feature may not arise if one follows a different approach to calculate the abundance of PBHs (in this regard, see, for example, Ref. [137]).

In the following section, we shall analyze the imprints of the inflationary scalar power spectrum and the dynamics of reheating on the spectral energy density of scalar-induced, secondary GWs. We shall also utilize the PTA data—in particular, the NANOGrav 15-year data [23–29]—to arrive at constraints on the reheating parameters. Notably, we shall also arrive at the constraints while ensuring the corresponding $f_{\text{PBH}}(M)$ lie within the observational bounds that we mentioned above.

3 Generation of scalar-induced secondary GWs and the PTA data

As is well known, primordial GWs are the transverse and traceless components of the tensor perturbations in the metric describing the FLRW universe. There can be different origins for GWs in the early universe. At the linear order in perturbation theory, the scalar and tensor perturbations evolve independently. However, the tensor perturbations at the second order can be sourced by the scalar perturbations at the first order. As a result, whenever the amplitudes of the scalar perturbations are enhanced on small scales so that the PBHs are formed abundantly, they induce tensor perturbations of significant strengths at the second order, often leading to a peak in the spectral density of GWs (see, for instance, Refs. [196, 197]). With the aim of explaining the PTA data, in this work, we focus on the generation GWs that are associated with the formation of PBHs during the phase of reheating described by a generic EoS. We shall consider an inflationary scalar power spectrum with a peak as given by Eq. (2.8) and compare the resulting spectral energy density of induced GWs with the NANOGrav 15-year data. Since we are interested in understanding the compatibility of the GW background generated during reheating with the detected NANOGrav 15-year signal, we shall assume a considerably low reheating temperature of $T_{\text{re}} \simeq 50$ MeV. Such an assumption ensures that the wave numbers with $k > k_{\text{re}}$ fall in the NANOGrav band of frequencies. Further, it is known that, when $w_{\text{re}} > 1/3$, a prolonged period of reheating can cause the spectral energy density of primary GWs (i.e. the GWs wave generated from the vacuum during inflation) to cross the so-called BBN bound. Later, we shall also utilize the bound to constrain the tensor-to-scalar ratio generated during inflation.

3.1 Spectral density of secondary GWs over wave numbers that re-enter during the phase of reheating

As we mentioned earlier, when the primordial scalar power spectrum is boosted on small scales to increase the number of PBHs formed, the enhanced scalar power also induces secondary GWs of significant strengths. In this section, we shall discuss the evaluation of the spectral energy density of the scalar-induced, secondary GWs generated during the phase of reheating and the epoch of radiation domination. We shall closely follow the formalism developed in the earlier efforts in this context (see, for instance, Refs. [20, 139, 140]).

Let h_{ij} represent the tensor perturbations at the second order and let $h_{\mathbf{k}}^\lambda$ denote the corresponding Fourier modes, where the superscript $\lambda = (+, \times)$ denotes the two types of polarization. In the presence of a source, say, $S_{\mathbf{k}}^\lambda$, the equation of motion governing the Fourier modes $h_{\mathbf{k}}^\lambda$ is given by

$$h_{\mathbf{k}}^{\lambda\prime\prime} + 2aH h_{\mathbf{k}}^{\lambda\prime} + k^2 h_{\mathbf{k}}^\lambda = S_{\mathbf{k}}^\lambda. \quad (3.1)$$

Recall that, in the absence of anisotropic stresses, at the first order, the scalar perturbations are described by the Bardeen potential Φ . In a background characterized by the constant EoS parameter w_{re} , the Fourier modes $\Phi_{\mathbf{k}}$ of the Bardeen potential satisfy the following equation of motion:

$$\Phi_{\mathbf{k}}'' + 3aH(1 + w_{\text{re}})\Phi_{\mathbf{k}}' + w_{\text{re}}k^2\Phi_{\mathbf{k}} = 0. \quad (3.2)$$

Since we are interested in the second-order tensor perturbations that are sourced by the first-order scalar perturbations, we can expect the source term $S_{\mathbf{k}}^\lambda$ to depend quadratically on the Fourier modes of the Bardeen potential $\Phi_{\mathbf{k}}$ [198–201]. At a time when the background is described by the constant EoS parameter w_{re} , the Bardeen potential is related to Fourier modes of the curvature perturbation $\mathcal{R}_{\mathbf{k}}$ generated during inflation as follows:

$$\Phi_{\mathbf{k}} = \frac{3(1 + w_{\text{re}})}{5 + 3w_{\text{re}}} T(k\eta) \mathcal{R}_{\mathbf{k}}, \quad (3.3)$$

where $T(k\eta)$ is the so-called transfer function that captures the time evolution of the Bardeen potential. One can show that the source term $S_{\mathbf{k}}^\lambda$ can be expressed as [199, 200]

$$S_{\mathbf{k}}^\lambda(\eta) = 4 \left[\frac{3(1 + w_{\text{re}})}{5 + 3w_{\text{re}}} \right]^2 \int \frac{d^3\mathbf{p}}{(2\pi)^{3/2}} \varepsilon^\lambda(\mathbf{k}, \mathbf{p}) f(p, q, \eta) \mathcal{R}_{\mathbf{p}} \mathcal{R}_{\mathbf{q}}, \quad (3.4)$$

where $\mathbf{q} = (\mathbf{k} - \mathbf{p})$ and, for convenience, we have introduced the quantity $\varepsilon^\lambda(\mathbf{k}, \mathbf{p}) = \varepsilon_{ij}^\lambda(\mathbf{k}) p^i p^j$. The quantity $f(p, q, \eta)$ involves combinations of the transfer function and its time derivative, and is given by

$$f(p, q, \eta) = 2T(p\eta)T(q\eta) + \frac{4}{3(1 + w_{\text{re}})} \left[T(p\eta) + \frac{T'(p\eta)}{aH} \right] \left[T(q\eta) + \frac{T'(q\eta)}{aH} \right]. \quad (3.5)$$

Also, it can be shown that

$$\varepsilon^+(\mathbf{k}, \mathbf{p}) = \frac{p^2}{\sqrt{2}} \sin^2\theta \cos(2\phi), \quad \varepsilon^\times(\mathbf{k}, \mathbf{p}) = \frac{p^2}{\sqrt{2}} \sin^2\theta \sin(2\phi), \quad (3.6)$$

where θ is the angle between the wave vectors \mathbf{k} and \mathbf{p} .

Let $G_k(\eta, \tilde{\eta})$ denote the Green's function that satisfies the differential equation

$$G_k'' + \left(k^2 - \frac{a''}{a} \right) G_k = \delta^{(1)}(\eta - \tilde{\eta}). \quad (3.7)$$

In such a case, the Fourier modes $h_{\mathbf{k}}^\lambda$ of the tensor perturbations at the second order, which are governed by Eq. (3.1), can be expressed in terms of the Green's function $G_k(\eta, \tilde{\eta})$ as follows:

$$h_{\mathbf{k}}^\lambda(\eta) = 4 \int \frac{d^3\mathbf{p}}{(2\pi)^{3/2}} \varepsilon^\lambda(\mathbf{k}, \mathbf{p}) I(p, q, \eta) \mathcal{R}_{\mathbf{p}} \mathcal{R}_{\mathbf{q}}, \quad (3.8)$$

where the kernel $I(p, q, \eta)$ is described by the integral

$$I(p, q, \eta) = \left[\frac{3(1 + w_{\text{re}})}{5 + 3w_{\text{re}}} \right]^2 \int \frac{d\tilde{\eta} a(\tilde{\eta})}{a(\eta)} G_k(\eta, \tilde{\eta}) f(p, q, \tilde{\eta}). \quad (3.9)$$

As is well known, if $u_k^1(\eta)$ and $u_k^2(\eta)$ are the two solutions to a second order, homogeneous differential equation, the Green's function associated with the inhomogeneous equation can be written as

$$G_k(\eta, \tilde{\eta}) = \frac{u_k^1(\eta) u_k^2(\tilde{\eta}) - u_k^1(\tilde{\eta}) u_k^2(\eta)}{u_k^{1'}(\tilde{\eta}) u_k^2(\tilde{\eta}) - u_k^1(\tilde{\eta}) u_k^{2'}(\tilde{\eta})}. \quad (3.10)$$

During the phase of reheating described by the constant EoS parameter w_{re} , the two homogeneous solutions to the differential equation (3.7) are given by $u_k^1(x) = \sqrt{x} J_{\alpha+1/2}(x)$ and $u_k^2(x) = \sqrt{x} Y_{\alpha+1/2}(x)$, where $x = k\eta$, $\alpha = (1 - 3w_{\text{re}})/(1 + 3w_{\text{re}})$, and $J_\nu(z)$ and $Y_\nu(z)$ are Bessel functions of the first and the second kind, respectively. On using these solutions, the Green's function $G_k(\eta, \tilde{\eta})$ can be written as

$$G_k(x, \tilde{x}) = -\frac{\pi}{2k} \sqrt{x\tilde{x}} [J_{\alpha+1/2}(x) Y_{\alpha+1/2}(\tilde{x}) - J_{\alpha+1/2}(\tilde{x}) Y_{\alpha+1/2}(x)]. \quad (3.11)$$

We now require the transfer function $T(k\eta)$ describing the Bardeen potential to construct the function $f(p, q, \eta)$ [cf. Eq. (3.5)]. During the phase of reheating, the general solution to Eq. (3.2) that governs the Bardeen potential can be expressed in terms of the Bessel functions $J_\nu(z)$ and $Y_\nu(z)$ as follows:

$$T(x) = x^{-(\alpha+3/2)} [C J_{\alpha+3/2}(\sqrt{w_{\text{re}}} x) + D Y_{\alpha+3/2}(\sqrt{w_{\text{re}}} x)], \quad (3.12)$$

where $x = k\eta$, and the coefficients C and D are to be determined by matching the transfer function and its time derivative with the earlier epoch. Note that the limit $x \ll 1$ corresponds to early times. In such a limit, since the second term in the above expression for $T(x)$ diverges, we shall set $D = 0$, i.e. we shall assume that there are no decaying solutions. Conventionally, the transfer function is chosen to be $T \rightarrow 1$ at large scales or, equivalently, when $x \ll 1$. Such a condition determines the value of the coefficient C to be $C = (2/\sqrt{w_{\text{re}}})^{\alpha+3/2} \Gamma(\alpha + 5/2)$ so that the transfer function is given by

$$T(x) = \left(\frac{2}{\sqrt{w_{\text{re}}} x} \right)^{\alpha+3/2} \Gamma\left(\alpha + \frac{5}{2}\right) J_{\alpha+3/2}(\sqrt{w_{\text{re}}} x). \quad (3.13)$$

On using this expression for the transfer function and after some simplification, we can express the function $f(p, q, \eta)$ as

$$f(u, v, x) = \frac{4^{\alpha+3/2}}{(2\alpha+3)(\alpha+2)} \Gamma^2\left(\alpha + \frac{5}{2}\right) (w_{\text{re}} u v x^2)^{-(\alpha+1/2)} \\ \times \left[J_{\alpha+1/2}(\sqrt{w_{\text{re}}} u x) J_{\alpha+1/2}(\sqrt{w_{\text{re}}} v x) \right]$$

$$+ \left(\frac{2 + \alpha}{1 + \alpha} \right) J_{\alpha+5/2}(\sqrt{w_{\text{re}}} u x) J_{\alpha+5/2}(\sqrt{w_{\text{re}}} v x) \Big], \quad (3.14)$$

where, for convenience, we have set $p = k v$ and $q = k u$.

Given the energy density of GWs at any given time, say, $\rho_{\text{GW}}(\eta)$, the corresponding spectral energy density is defined as $\rho_{\text{GW}}(k, \eta) = d\rho_{\text{GW}}(\eta)/d \ln k$. The spectral energy density of the secondary GWs can be expressed as

$$\rho_{\text{GW}}(k, \eta) = \frac{M_{\text{Pl}}^2}{8} \left(\frac{k}{a} \right)^2 \overline{\mathcal{P}_h(k, \eta)}, \quad (3.15)$$

where $\mathcal{P}_h(k, \eta)$ denotes the power spectrum of the GWs generated due to the second order scalar perturbations and is defined through the relation

$$\langle h_{\mathbf{k}}^\lambda(\eta) h_{\mathbf{k}'}^{\lambda'}(\eta) \rangle = \frac{2\pi^2}{k^3} \mathcal{P}_h(k, \eta) \delta^{(3)}(\mathbf{k} + \mathbf{k}') \delta^{\lambda\lambda'}. \quad (3.16)$$

We should clarify that the spectrum $\mathcal{P}_h(k, \eta)$ is to be evaluated at late times when the wave numbers of interest are well inside the Hubble radius and the overbar denotes the average over the oscillations that occur on small time scales.

Since the Fourier modes $h_{\mathbf{k}}^\lambda$ depend quadratically on the Fourier modes $\mathcal{R}_{\mathbf{k}}$ of the inflationary curvature perturbations [cf. Eq. (3.8)], evidently, the power spectrum $\mathcal{P}_h(k, \eta)$ will involve products of four $\mathcal{R}_{\mathbf{k}}$. On using Wick's theorem, which applies to Gaussian random variables, we can express the spectral density $\rho_{\text{GW}}(k, \eta)$ during reheating as [20, 139, 140]

$$\begin{aligned} \rho_{\text{GW}}(k, \eta) &= \frac{M_{\text{Pl}}^2}{2} \left(\frac{k}{a} \right)^2 \int_0^\infty dv \int_{|1-v|}^{1+v} du \left[\frac{4v^2 - (1 + v^2 - u^2)^2}{4uv} \right]^2 \\ &\times \overline{I^2(u, v, x)} \mathcal{P}_{\mathcal{R}}(ku) \mathcal{P}_{\mathcal{R}}(kv), \end{aligned} \quad (3.17)$$

where the kernel $I(u, v, x)$ can be expressed as

$$\begin{aligned} I(u, v, x) &= \frac{4^\alpha (2 + \alpha) \pi}{(3 + 2\alpha) (w_{\text{re}} u v x)^{(\alpha+1/2)}} \Gamma^2 \left(\alpha + \frac{3}{2} \right) \\ &\times [\mathcal{I}_J(u, v, x) Y_{\alpha+1/2}(x) - \mathcal{I}_Y(u, v, x) J_{\alpha+1/2}(x)] \end{aligned} \quad (3.18)$$

with the functions $\mathcal{I}_J(u, v, x)$ and $\mathcal{I}_Y(u, v, x)$ being described by the integrals

$$\begin{aligned} \mathcal{I}_J(u, v, x) &= \int_0^x d\tilde{x} \tilde{x}^{-\alpha+1/2} J_{\alpha+1/2}(\tilde{x}) \left[J_{\alpha+1/2}(\sqrt{w_{\text{re}}} u \tilde{x}) J_{\alpha+1/2}(\sqrt{w_{\text{re}}} v \tilde{x}) \right. \\ &\quad \left. + \left(\frac{2 + \alpha}{1 + \alpha} \right) J_{\alpha+5/2}(\sqrt{w_{\text{re}}} u \tilde{x}) J_{\alpha+5/2}(\sqrt{w_{\text{re}}} v \tilde{x}) \right], \end{aligned} \quad (3.19a)$$

$$\begin{aligned} \mathcal{I}_Y(u, v, x) &= \int_0^x d\tilde{x} \tilde{x}^{-\alpha+1/2} Y_{\alpha+1/2}(\tilde{x}) \left[J_{\alpha+1/2}(\sqrt{w_{\text{re}}} u \tilde{x}) J_{\alpha+1/2}(\sqrt{w_{\text{re}}} v \tilde{x}) \right. \\ &\quad \left. + \left(\frac{2 + \alpha}{1 + \alpha} \right) J_{\alpha+5/2}(\sqrt{w_{\text{re}}} \tilde{x}) J_{\alpha+5/2}(\sqrt{w_{\text{re}}} \tilde{x}) \right]. \end{aligned} \quad (3.19b)$$

While these integrals are difficult to calculate analytically for a finite x , they can be evaluated in the limit $x \rightarrow \infty$. It can be shown that, in such a limit, the integrals $\mathcal{I}_J(u, v, x)$ and

$\mathcal{I}_Y(u, v, x)$ can be expressed as

$$\lim_{x \rightarrow \infty} \mathcal{I}_J(u, v, x) = \frac{\pi}{2} \frac{(w_{\text{re}}/2)^{\alpha-1/2}}{\pi \sqrt{\pi} u v} \Theta \left(u + v - \frac{1}{\sqrt{w_{\text{re}}}} \right) Z^\alpha \left[P_\alpha^{-\alpha}(y) + \left(\frac{2+\alpha}{1+\alpha} \right) P_{\alpha+2}^{-\alpha}(y) \right], \quad (3.20a)$$

$$\begin{aligned} \lim_{x \rightarrow \infty} \mathcal{I}_Y(u, v, x) = & -\frac{(w_{\text{re}}/2)^{\alpha-1/2}}{\pi \sqrt{\pi} u v} \left\{ \Theta \left(u + v - \frac{1}{\sqrt{w_{\text{re}}}} \right) Z^\alpha \left[Q_\alpha^{-\alpha}(y) + \left(\frac{2+\alpha}{1+\alpha} \right) Q_{\alpha+2}^{-\alpha}(y) \right] \right. \\ & \left. - \Theta \left(\frac{1}{\sqrt{w_{\text{re}}}} - u - v \right) \tilde{Z}^\alpha \left[\mathcal{Q}_\alpha^{-\alpha}(\tilde{y}) + 2 \left(\frac{2+\alpha}{1+\alpha} \right) \mathcal{Q}_{\alpha+2}^{-\alpha}(\tilde{y}) \right] \right\}, \quad (3.20b) \end{aligned}$$

where

$$y = \left(\frac{u^2 + v^2 - 1/w_{\text{re}}}{2uv} \right), \quad Z^2 = 4u^2v^2(1-y^2), \quad \tilde{y} = -y, \quad \tilde{Z}^2 = -Z^2. \quad (3.21)$$

In the above expressions, the functions $P_\nu^\mu(z)$ and $Q_\nu^\mu(z)$ are referred to as the Legendre polynomials on the cut, and $\mathcal{Q}_\nu^\mu(z)$ is the associated Legendre polynomial (we would refer the reader to Ref. [139] for further details). In the late time limit of our interest, i.e. when $x \gg 1$, the Bessel functions in Eq. (3.18) behave as $J_\nu(x) = \sqrt{2/(\pi x)} \cos[x - (2\nu + 1)\pi/4]$ and $Y_\nu(x) = \sqrt{2/(\pi x)} \sin[x - (2\nu + 1)\pi/4]$. As a result, when we square $I(u, v, x)$ and average over the oscillations, the square of the sine and the cosine functions will be replaced by the average value of 1/2, while the cross term will vanish. Therefore, we finally obtain that

$$\begin{aligned} \lim_{x \gg 1} \overline{I^2(u, v, x)} \simeq & \frac{4^\alpha}{2w_{\text{re}}^2} \left(\frac{2+\alpha}{3+2\alpha} \right)^2 \Gamma^4 \left(\alpha + \frac{3}{2} \right) (uvx)^{-2(\alpha+1)} \\ & \times \left\{ \Theta \left(u + v - \frac{1}{\sqrt{w_{\text{re}}}} \right) Z^{2\alpha} \left[P_\alpha^{-\alpha}(y) + \left(\frac{2+\alpha}{1+\alpha} \right) P_{\alpha+2}^{-\alpha}(y) \right]^2 \right. \\ & + \frac{4}{\pi^2} \Theta \left(u + v - \frac{1}{\sqrt{w_{\text{re}}}} \right) Z^{2\alpha} \left[Q_\alpha^{-\alpha}(y) + \left(\frac{2+\alpha}{1+\alpha} \right) Q_{\alpha+2}^{-\alpha}(y) \right]^2 \\ & \left. + \frac{4}{\pi^2} \Theta \left(\frac{1}{\sqrt{w_{\text{re}}}} - u - v \right) \tilde{Z}^{2\alpha} \left[\mathcal{Q}_\alpha^{-\alpha}(\tilde{y}) + 2 \left(\frac{2+\alpha}{1+\alpha} \right) \mathcal{Q}_{\alpha+2}^{-\alpha}(\tilde{y}) \right]^2 \right\} \quad (3.22) \end{aligned}$$

and, with this quantity in hand, we can evaluate the integrals over u and v in Eq. (3.17), say, numerically, to eventually arrive at $\rho_{\text{GW}}(k, \eta)$. From the above expression for the average of $I^2(u, v, x)$ and the factor of a^{-2} in Eq. (3.17), it should be clear that $\rho_{\text{GW}}(k, \eta)$ behaves as a^{-4} . Such a behavior is over wave numbers that are well inside the Hubble radius at late times. We should add that the $\rho_{\text{GW}}(k, \eta)$ we have obtained above applies to wave numbers $k_{\text{re}} < k < k_e$, where, recall that, k_{re} denotes the wave number that re-enters the Hubble radius at the end of the phase of reheating, while k_e is the wave number that leaves the Hubble radius at the end of inflation (or, equivalently, re-enters at the start of reheating).

Note that, since, in our analysis, we assume that the wave numbers near the peak in the scalar power spectrum re-enter during the phase of reheating (i.e. they lie in the range $k_{\text{re}} < k < k_e$), the dominant contribution to the spectral density of secondary GWs can be expected to arise from the phase. The phase of reheating will be followed by the epoch of radiation domination. The secondary GWs generated over $k_{\text{re}} < k < k_e$ during reheating will freely propagate during radiation domination. In the following section, we shall discuss the generation of secondary GWs during the epoch of radiation domination.

3.2 Spectral density of secondary GWs over wave numbers that re-enter during radiation domination

Let us now turn to wave numbers $k < k_{\text{re}}$ that re-enter the Hubble radius during the epoch of radiation domination. Given that the radiation-dominated epoch was preceded by the phase of reheating, the general solution for the transfer function $T(x)$ for the scalar perturbations at the first order can be written as [202]

$$T(x) = \frac{3\sqrt{3}}{x - \alpha x_{\text{re}}/(1 + \alpha)} \left\{ A(x_{\text{re}}) j_1 \left[\frac{1}{\sqrt{3}} \left(x - \frac{\alpha}{1 + \alpha} x_{\text{re}} \right) \right] + B(x_{\text{re}}) y_1 \left[\frac{1}{\sqrt{3}} \left(x - \frac{\alpha}{1 + \alpha} x_{\text{re}} \right) \right] \right\}, \quad (3.23)$$

where $j_1(z)$ and $y_1(z)$ are the spherical Bessel functions of the first and second kind, and $x_{\text{re}} = k \eta_{\text{re}}$. Note that the above transfer function accounts for the redefinition of the scale factor due to the presence of a reheating phase, in contrast to the case of instantaneous reheating [see $a(\eta)$ in Eq. (2.6)]. This aspect needs to be taken into account carefully while deriving the kernel $I(u, v, x)$ for the epoch of radiation domination. Needless to say, the effect of this redefinition becomes unimportant for wave numbers such that $k \ll k_{\text{re}}$, i.e. modes which re-enter during the time $\eta \gg \eta_{\text{re}}$.

There is an important point that we need to clarify at this stage of our discussion. Consider a sharply peaked primordial scalar power spectrum with its maximum at k_{peak} . If the wave number k_{peak} re-enters during the phase of reheating and, if $k_{\text{re}} \simeq k_{\text{peak}}$, then, due to the nature of the convolution integral describing the spectral density of secondary GWs, the GWs generated over $k \lesssim k_{\text{re}}$ can also be affected by the phase of reheating (in this regard, see Refs. [20, 140]). Such an effect can also arise in the scenario that we consider in this work. It is precisely to avoid such an effect that we have assumed a rather low reheating temperature, which leads to a low value for k_{re} thereby ensuring that $k_{\text{re}} \ll k_{\text{peak}}$. In such a situation, the effects of the modification to the kernel $I(u, v, x)$ during radiation domination due to the redefined scale factor do not play a significant role in estimation of the spectral density of secondary GWs.

The more general form of the kernel during radiation domination—which accounts for the prior phase of reheating—can be derived with x_{re} redefined as $x_{\text{re}}/2 \rightarrow [\alpha/(1 + \alpha)] x_{\text{re}}$ (in this regard, see Ref. [203], App. A). Moreover, the constants $A(x_{\text{re}})$ and $B(x_{\text{re}})$ in the transfer function (3.23) above can be determined by matching the Bardeen potential and its time derivative at η_{re} . Clearly, the resulting kernel will reduce to the standard kernel in the epoch of radiation domination for wave numbers $k \ll k_{\text{re}}$ that re-enter much later than η_{re} . In the late time limit, i.e. as $x \rightarrow \infty$, we can write the kernel during radiation domination as [196, 197]

$$\lim_{x \rightarrow \infty} \overline{I^2(v, u, x)} = \frac{1}{2} \left[\frac{3(u^2 + v^2 - 3)}{4u^3 v^3 x} \right]^2 \left\{ \left[4uv + (u^2 + v^2 - 3) \log \left| \frac{3 - (u+v)^2}{3 - (u-v)^2} \right| \right]^2 + \Theta(u + v - \sqrt{3}) \pi^2 (u^2 + v^2 - 3)^2 \right\}. \quad (3.24)$$

In our scenario, which involves a sharply ascending scalar power spectrum with a peak that re-enters the Hubble radius well before the epoch of radiation domination, we can make use of this kernel in Eq. (3.17) without losing any accuracy in the estimate of the spectral density of secondary GWs over wave numbers such that $k \ll k_{\text{re}} < k_{\text{peak}}$.

The dimensionless spectral energy density parameter $\Omega_{\text{GW}}(k, \eta)$ associated with $\rho_{\text{GW}}(k, \eta)$ is defined with respect to the critical density at the time, viz. $\rho_{\text{cr}}(\eta)$, as

$$\Omega_{\text{GW}}(k, \eta) = \frac{\rho_{\text{GW}}(k, \eta)}{\rho_{\text{cr}}(\eta)} = \frac{\rho_{\text{GW}}(k, \eta)}{3 M_{\text{Pl}}^2 H^2}. \quad (3.25)$$

The present-day, dimensionless spectral energy density of secondary GWs can be expressed in terms of the quantity $\Omega_{\text{GW}}(k, \eta)$ as follows:

$$\Omega_{\text{GW}}(k) h^2 = c_g \Omega_r h^2 \Omega_{\text{GW}}(k, \eta) = \frac{c_g \Omega_r h^2}{24} \left(\frac{k}{a H} \right)^2 \overline{\mathcal{P}_h(k, \eta)}, \quad (3.26)$$

where $c_g = (g_k/g_0) (g_{s,0}/g_{s,k})^{4/3}$, with $(g_k, g_{s,k})$ and $(g_0, g_{s,0})$ denoting the effective number of relativistic degrees of freedom associated with the energy density of radiation and entropy when the wave number k re-enters the Hubble radius and today, respectively.

In Fig. 2, we have plotted the dimensionless spectral density Ω_{GW} of the primary (in this context, see Sec. 3.4) and secondary GWs as a function of the frequency f . In the figure, we have also included the projected sensitivity curves of different current and forthcoming GW observatories such as PTA, Square Kilometre Array (SKA) [204], LISA [205], DECIGO [206, 207], BBO [208–210], MAGIS-100 [196, 211], advanced LIGO + Virgo (LVK) [212, 213], ET [214], and CE [215]. We should point out that the sensitivity curves have been arrived at by assuming a power law for the spectral density of GWs and integrating the noise data over a range of frequencies and observation time. The sensitivity curves indicate in a simple way whether the spectral densities we have calculated will be detected by the GW observatories. Note that, in plotting the dimensionless spectral energy densities of the primary and secondary GWs, we have fixed the reheating temperature to be $T_{\text{re}} \simeq 50$ MeV. Moreover, in the case of the secondary GWs, we have assumed that the scalar power spectrum has a broken power law form, as given in Eq. (2.8). Further, we have chosen that the peak in the scalar power spectrum to be at $k_{\text{peak}} = 10^{7.5} \text{ Mpc}^{-1}$, and we have assumed that $n_0 = -2$. The reason for choosing these values of T_{re} and k_{peak} is to effectively constrain w_{re} with the aid of the PTA data. Recall that, we have assumed a sudden transition from the phase of reheating to the era of radiation domination. We have chosen the above-mentioned parameters such that the wave number k_{re} occurs before the range of frequencies that the PTAs are sensitive to. In the figure, we have plotted the quantity $\Omega_{\text{GW}}(f)$ for the following five values of the parameter that describes the EoS during reheating: $w_{\text{re}} = (1/10, 1/3, 2/5, 3/5, 9/10)$. It is clear from the figure that, as w_{re} increases, the height of the peak in the secondary $\Omega_{\text{GW}}(f)$ also increases and the bump-like feature around the peak is flattened. It is also evident from the figure that, for all values of w_{re} , prior to the peak, the spectral density of the secondary GWs behaves as expected for wave numbers that re-enter the Hubble radius during the epoch of radiation domination. Beyond the peak, the spectral density of the secondary GWs decreases in different manner for different values of w_{re} . As w_{re} is increased from zero, $\Omega_{\text{GW}}(f)$ falls less and less and it becomes nearly constant for $w_{\text{re}} = 1/3$, and starts increasing again for $w_{\text{re}} > 1/3$. This happens due to the relative redshift between the background and GWs. The second rise in the spectral density of secondary GWs can also be detected by observatories such as LISA, DECIGO, and BBO. Hence, the presence of a double peak can indicate an EoS with $w_{\text{re}} > 1/3$.

There are a couple of related points regarding Fig. 2 that require further emphasis. In the figure, we have plotted the spectral energy densities of the primary and secondary GWs up to

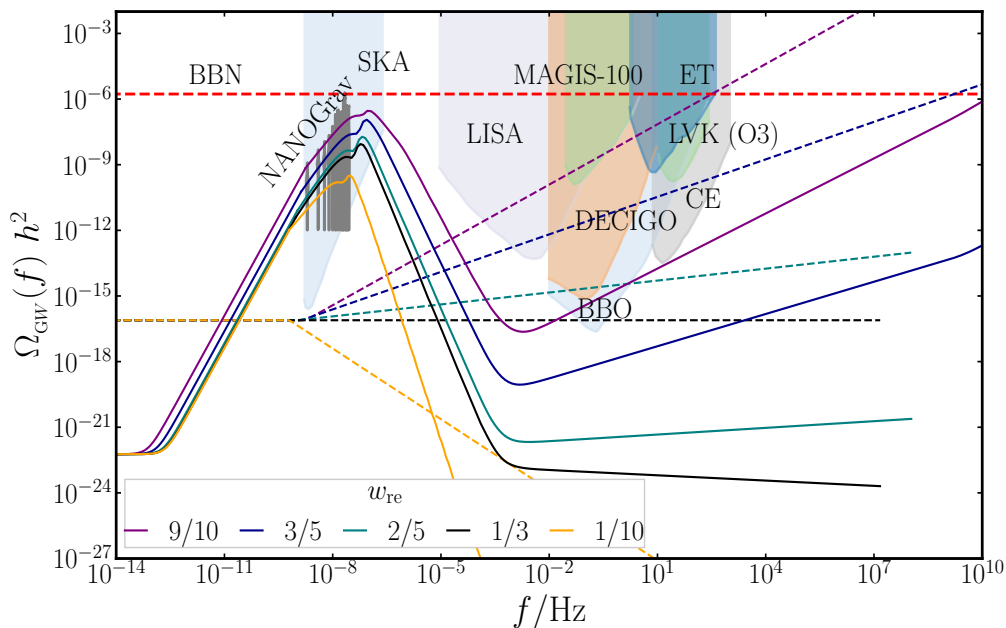


Figure 2. The dimensionless spectral energy density Ω_{GW} of both the primary (as dashed curves) and secondary (as solid curves) GWs arising in the scenario of interest are plotted as a function of the frequency f . We have plotted the spectral energy densities up to the frequency corresponding to the wavenumber k_e which leaves the Hubble radius at the end of inflation. In plotting the spectral density of secondary GWs, we have chosen the parameters of the primordial scalar power spectrum [cf. Eq. (2.8)] to be $\log_{10} A_0 = -1.5$, $\log_{10}(k_{\text{peak}}/\text{Mpc}^{-1}) = 7.5$ and $n_0 = -2$. We have set the reheating temperature to be $T_{\text{re}} = 50 \text{ MeV}$ and have plotted the results for the following values of the EoS parameter during reheating: $w_{\text{re}} = (1/10, 1/3, 2/5, 3/5, 9/10)$. We should mention that the spectral energy densities of the primary GWs are plotted corresponding to the maximum value of the tensor-to-scalar ratio allowed by the CMB data, viz. $r = 0.036$ [117], which sets the upper bound on the energy scale of inflation (in this context, see our discussion in Sec. 3.4). In the figure, we have also indicated the so-called BBN bound (as the dashed red line), which limits the total energy density of relativistic fields during the epoch of radiation domination.

the frequency corresponding to the wavenumber k_e , where, recall that, k_e is the wavenumber that leaves the Hubble radius at the end of inflation. Note that the Fourier modes with wavenumbers larger than k_e always stay within the Hubble radius and hence they do not contribute to the energy density of GWs (for a discussion in this regard, see, for example, Refs. [216, 217]). It is clear from the figure that, for $w_{\text{re}} = 9/10$, the spectral energy density of primary GWs crosses the sensitivity curve of LVK as well as the BBN bound from ΔN_{eff} . Whereas, for $w_{\text{re}} = 3/5$, the spectral energy density of the primary GWs crosses only the BBN bound. Based on the fact that LVK did not observe a SGWB [22], we can exclude the spectral energy densities passing through it. Therefore, for the tensor-to-scalar ratio of $r = 0.036$, we can rule out the possibility of a prolonged reheating phase with either $w_{\text{re}} = 9/10$ or $w_{\text{re}} = 3/5$. But, a smaller value of r (or, equivalently, a lower inflationary energy scale) would still remain compatible with such reheating histories. These suggest that, for a given energy scale of inflation, BBN and LVK can also be used to constrain the parameters that characterize the epoch of reheating. In fact, blue-tilted inflationary spectra can be constrained by LVK very

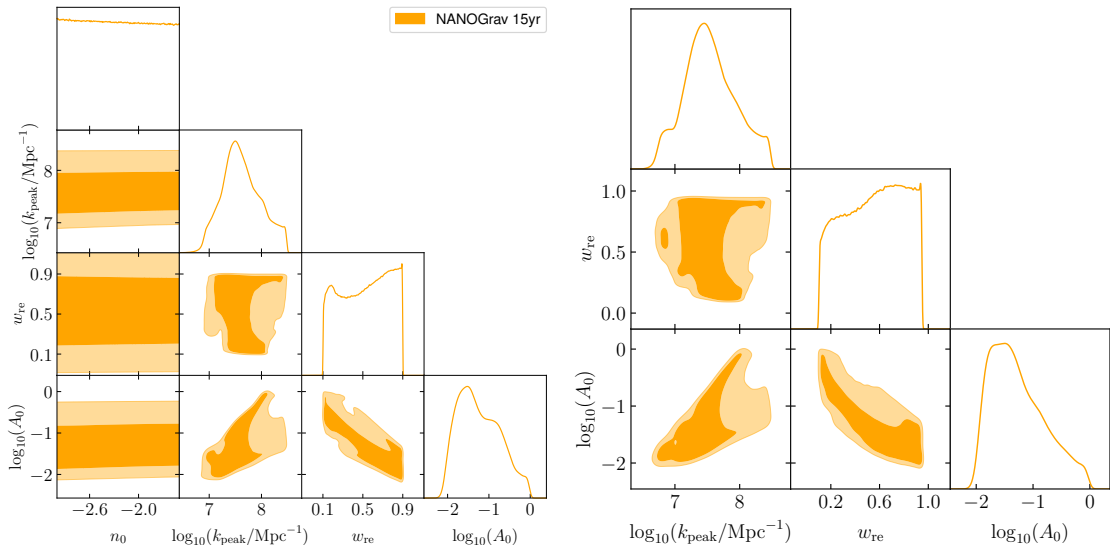


Figure 3. We have plotted the marginalized posterior distributions of the parameters that have been arrived at upon comparing the models **R4pF** (on the left) and **R3pF** (on the right) with the NANOGrav 15-year data. Note that, in both the models, while the data constrains the parameters A_0 and k_{peak} fairly well (as is suggested by the peaks in their posterior distributions), the constraints on the parameters w_{re} and n_0 (in the case of the model **R4pF**) are rather weak. In fact, in the case of n_0 , the posterior distribution is flat over the range of priors that we have worked with [cf. Tab. 1].

effectively. However, we should point out that, if we consider a flat or red-tilted inflationary tensor power spectrum, the bound from ΔN_{eff} provides a stronger constraint on primary GWs than LVK.

3.3 Comparison with the NANOGrav 15-year data

In this section, we scan our parameter space to find the region of the space that optimally fits the PTA data. We shall further examine whether the optimal values for the parameters we obtain are consistent with the available constraints on $f_{\text{PBH}}(M)$.

We use the NANOGrav 15-year data [23, 218] and, to arrive at the best-fit parameters, we carry out a Markov-Chain Monte Carlo (MCMC) analysis with the help of `PTArcade` [219] in the `ceffy1` mode. Our initial search consists of four parameters, viz. the three parameters $(A_0, k_{\text{peak}}, n_0)$ that describe the inflationary scalar power spectrum [cf. Eq. (2.8)] and the parameter w_{re} that describes the EoS during reheating. As we discussed earlier, our method to calculate the spectral density of secondary GWs lose the desired precision around wave numbers that re-enter the Hubble radius close to the time of transition from the phase of reheating to the epoch of radiation domination. To circumvent this limitation, we choose the reheating temperature to be $T_{\text{re}} = 50 \text{ MeV}$, so that the frequency corresponding to k_{re} always remains much smaller than the frequency range probed by NANOGrav. First, we run `PTArcade` to sample over the four parameters $(A_0, k_{\text{peak}}, n_0, w_{\text{re}})$ and, for convenience, we refer to this model as **R4pF**. In Tab. 1, we have listed the priors we work with and the mean values we have obtained from the run. And, in Fig. 3, we have illustrated the resulting marginalized posterior distributions (known, popularly, as the triangular plots). It is evident from the posterior distributions that the PTA data does not constrain the parameter n_0 . Such a result should not be surprising since the NANOGrav 15-year data only favors an ascending

Model	Parameter	Prior	Mean value		
R4pF	$\log_{10}\left(\frac{k_{\text{peak}}}{\text{Mpc}^{-1}}\right)$	[6, 9]	$7.62^{+0.35}_{-0.41}$		
	$\log_{10}(A_0)$	[-3, 0]	$-1.23^{+0.38}_{-0.66}$		
	w_{re}	[0.1, 0.9]	0.52 ± 0.23		
	n_0	[-3.0, -1.5]	-2.26 ± 0.43		
R3pF	$\log_{10}\left(\frac{k_{\text{peak}}}{\text{Mpc}^{-1}}\right)$	[6, 9]	$7.54^{+0.36}_{-0.44}$		
	$\log_{10}(A_0)$	[-3, 0]	$-1.26^{+0.26}_{-0.64}$		
	w_{re}	[0.1, 0.9]	$0.55^{+0.39}_{-0.14}$		
			$0.5 \delta_{\text{c}}^{\text{an}}$	$\delta_{\text{c}}^{\text{an}}$	$1.5 \delta_{\text{c}}^{\text{an}}$
R3pB	$\log_{10}\left(\frac{M}{M_{\odot}}\right)$	[-6, 3.5]	$-0.12^{+0.28}_{-0.15}$	$-1.18^{+0.35}_{-0.39}$	$-1.85^{+0.49}_{-0.30}$
	$\log_{10}(f_{\text{PBH}})$	[-20, 0]	$-0.67^{+0.68}_{-0.16}$	$-6.6^{+6.5}_{-1.9}$	$-10.2^{+8.2}_{-9.6}$
	w_{re}	[0.1, 0.9]	$0.78^{+0.11}_{-0.030}$	$0.66^{+0.23}_{-0.19}$	0.55 ± 0.17
R2pB	$\log_{10}\left(\frac{M}{M_{\odot}}\right)$	[-6, 3.5]	$-0.24^{+0.38}_{-0.45}$	$-1.60^{+0.16}_{-0.14}$	$-2.45^{+0.20}_{-0.13}$
	w_{re}	[0.1, 0.9]	$0.77^{+0.13}_{-0.038}$	0.59 ± 0.16	$0.464^{+0.095}_{-0.25}$

Table 1. We have listed the parameters in the four models we consider, viz. R4pF, R3pF, R3pB and R2pB, the priors we have worked with, and the mean values we have obtained upon comparison of the models with the NANOGrav 15-year data. We should mention that, in our analysis, we have assumed the priors to be uniform.

spectral density of GWs $\Omega_{\text{GW}}(f)$ over the range of frequencies it is sensitive to. In fact, a nearly scale-invariant spectrum is ruled out beyond $3\text{-}\sigma$ by the data. This, in turn, implies that the data constrains the rising part of the inflationary scalar power spectrum prior to the peak. We should add that, in the model R4pF, we do not compute the mass fraction $f_{\text{PBH}}(M)$ or do not take into account the constraints on the abundance of PBHs. It would be interesting to explore the effects of changing n_0 on the PBH mass fraction and the resulting constraints from the NANOGrav 15-year data, particularly when one takes into account the dependence of δ_{c} on the shape of the inflationary scalar power spectrum [162, 181]. However, for the present work, we shall assume the effects of changing n_0 to be negligible and, as the next step, we fix the value of n_0 to consider a model that involves only the three parameters $(A_0, k_{\text{peak}}, w_{\text{re}})$. We refer to this three parameter model as R3pF. As before, in Tab. 1, we have listed the priors and best-fit values arrived at upon comparison with the NANOGrav 15-year data. Also, in Fig. 3, we have illustrated the marginalized posterior distributions that we have obtained.

Until this point, we have only compared the two models R4pF and R3pF with the NANOGrav 15-year data. We also need to make sure that the best-fit parameters that describe the scalar power spectrum (in particular, the amplitude A_0) does not lead to the overproduction of PBHs, an issue that has been encountered recently in similar contexts in the literature (in this regard, see, for instance, Refs. [31, 40, 134, 135]). To ensure that there is no excessive production of PBHs, we carry out fresh runs wherein we directly sample the

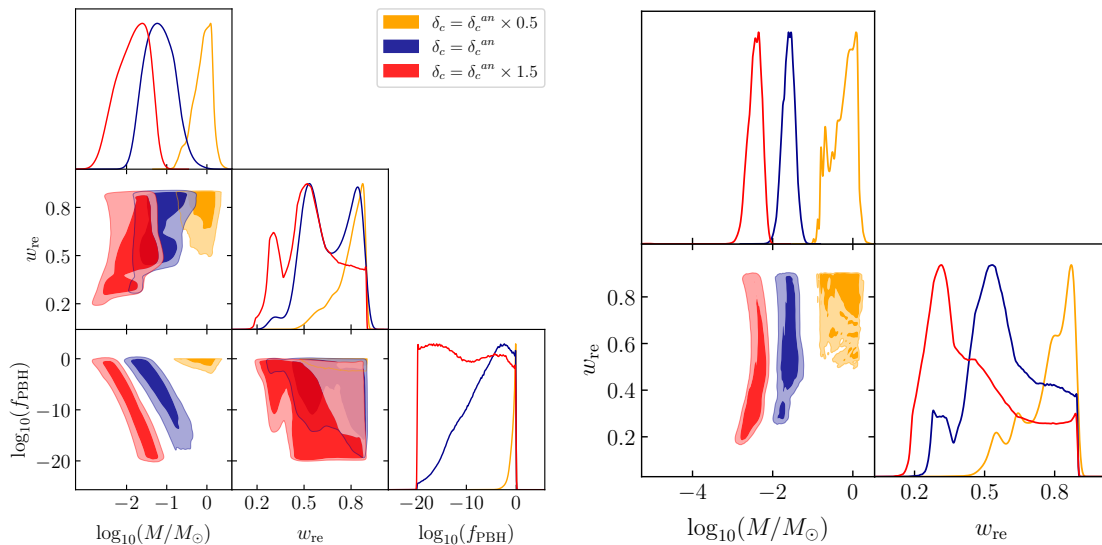


Figure 4. As in the previous figure, we have plotted the marginalized posterior distributions of the parameters that have been arrived at upon comparing the models R3pB (on the left) and R2pB (on the right) with the NANOGrav 15-year data. A notable feature of these results is that, for lower values of δ_c , the data prefers higher values of M_{PBH} and w_{re} .

parameters that describe the PBHs, viz. M and f_{PBH} , along with the reheating parameter w_{re} . In other words, for a given set of parameters $(A_0, k_{\text{peak}}, w_{\text{re}})$, we calculate the quantity $f_{\text{PBH}}(M)$ and ensure that it is always less than unity. As we discussed in Sec. 2.2, it is the uncertainties related to the collapse of PBHs that play an important role in determining the value of the critical density contrast δ_c . In order to understand the effects of the uncertainties on our results, apart from the value of the critical density δ_c^{an} given by the analytical expression (2.15), we also scan the parameter space for a smaller ($\delta_c = 0.5 \delta_c^{\text{an}}$) and a higher ($\delta_c = 1.5 \delta_c^{\text{an}}$) value of δ_c . We refer to the model as R3pB. We indeed find that the change in the value of δ_c has a strong effect on the optimal or best-fit values. Such a conclusion should be evident from Tab. 1 wherein we have listed the optimal values, and the posterior distributions we have plotted in Fig. 4. The effect is particularly clear from the posterior distribution for f_{PBH} plotted in Fig. 4. Note that, for $\delta_c = 0.5 \delta_c^{\text{an}}$, the PBHs are overproduced for almost the entire range of the reheating parameter w_{re} , barring values close to unity. This is understandable as a larger w_{re} implies a larger δ_c^{an} . In complete contrast, for $\delta_c = 1.5 \delta_c^{\text{an}}$, the entire range of f_{PBH} we consider is allowed with equal probability for almost all values of w_{re} . If we choose the intermediate value of $\delta_c = \delta_c^{\text{an}}$, we find that the condition that PBHs are not overproduced does not significantly constrain w_{re} . However, we do find that the data favors $w_{\text{re}} \gtrsim 0.5$. Moreover, the posterior distribution for f_{PBH} shows a monotonic rise with the increasing f_{PBH} .

The condition that $f_{\text{PBH}} < 1$ is the theoretical bound that exists on all mass scales. But, there are also mass-dependent constraints that need to be taken into account in the range of optimal PBH masses that we obtain. As illustrated in Fig. 5, in the range of PBH masses of our interest, the constraints through micro-lensing from HSC OGLE [193, 194, 220] and the constraints from the Planck-2018 CMB data [10] play the most important role. Therefore, in our final run, we fix $f_{\text{PBH}}(M)$ to the maximum possible value allowed by the constraints from the different micro-lensing observations (as shown in Fig. 5), and scan only over the parameters M and w_{re} . We refer to this model as R2pB. Further, we perform a Bayesian

Model X	Model Y	BF _{Y,X}		
		$\delta_c = 0.5 \delta_c^{\text{an}}$	$\delta_c = \delta_c^{\text{an}}$	$\delta_c = 1.5 \delta_c^{\text{an}}$
SMBHBs	R2pB	$1.7 \pm .06$	260.04 ± 19.21	350.61 ± 27.36

Table 2. We have listed the Bayesian factors BF_{Y,X} that we have obtained for the model R2pB which invokes primordial physics as the source of the SGWB observed by the NANOGrav 15-year data, when compared to the astrophysical scenario of SMBHBs. Bayesian factors BF_{Y,X} that far exceed unity indicate strong evidence for the model Y with respect to the model X. Clearly, when $\delta_c = \delta_c^{\text{an}}$ and $\delta_c = 1.5 \delta_c^{\text{an}}$, the NANOGrav 15-year data strongly favors the model R2pB when compared to the model of SMBHBs.

analysis of the two-parameter model. As in the case of the model R3pB, we allow δ_c to take three different values and compare them with the PTA data. And, as in the earlier model, we find clear distinction in the optimal parameter range in these different cases.

To carry out a Bayesian analysis of the two-parameter model R2pB against the NANOGrav 15-year data, we make use of PTArcade [219] in the enterprise [221] mode without the Hellings and Downs [222] correction. Let \mathcal{D} denote the PTA data and let θ denote the parameters describing our model. As is well known, in such a case, the posterior distribution $\mathcal{P}(\theta|\mathcal{D})$ is given by

$$\mathcal{P}(\theta|\mathcal{D}) = \frac{\mathcal{P}(\mathcal{D}|\theta) \mathcal{P}(\theta)}{\mathcal{P}(\mathcal{D})}, \quad (3.27)$$

where $\mathcal{P}(\theta)$ is the distribution of the priors on the parameters involved, and $\mathcal{P}(\mathcal{D})$ denotes the marginalized likelihood. We obtain the marginalized likelihood in support of model Y and utilize it to evaluate the Bayesian factor against a reference model X through the relation

$$\text{BF}_{Y,X} \equiv \frac{\mathcal{P}(\mathcal{D}|Y)}{\mathcal{P}(\mathcal{D}|X)}. \quad (3.28)$$

For the reference model X, we choose the source of GWs to be the merging of SMBHBs. In PTArcade and enterprise [221], we choose the `smbhb=True` and `bhb_th_prior=True` options, which assumes two-dimensional Gaussian priors for the parameters A_{BHB} and γ_{BHB} of the SMBHBs [30, 219]. We have listed the Bayesian factors for the model R2pB corresponding to the three different choices of δ_c in Tab. 2. It is clear from the table that, when $\delta_c = 0.5 \delta_c^{\text{an}}$, the model R2pB performs only slightly better than the model of SMBHBs. However, when $\delta_c = \delta_c^{\text{an}}$ and $\delta_c = 1.5 \delta_c^{\text{an}}$, our comparison with the NANOGrav’s 15-year data finds strong Bayesian evidence in favor of the scenario wherein PBHs are formed during reheating, resulting in the generation of secondary GWs rather than the SMBHB model.

In Fig. 5, we have plotted the spectral density of secondary GWs $\Omega_{\text{GW}}(f)$ that correspond to the best-fit values of the parameters in the four models R4pF, R3pF, R3pB and R2pB, which we have considered. In Fig. 6, we have plotted the corresponding inflationary scalar power spectra $\mathcal{P}_{\mathcal{R}}(k)$ and fraction of PBHs $f_{\text{PBH}}(M)$ that constitute the energy density of cold dark matter today. The most important effect in the latter two models is the shift in the set of optimal parameters upon the implementation of condition for the formation of PBHs. The latter models prefer comparatively higher values of w_{re} and δ_c . As should be clear from the plots of $f_{\text{PBH}}(M)$ in Fig. 6, the two original two models, viz. R4pF and R3pF, though they lead to a good fit to the NANOGrav 15-year data, they overproduce PBHs. However, as should be evident from the figure, the models R3pB and R2pB are consistent $f_{\text{PBH}}(M) < 1$

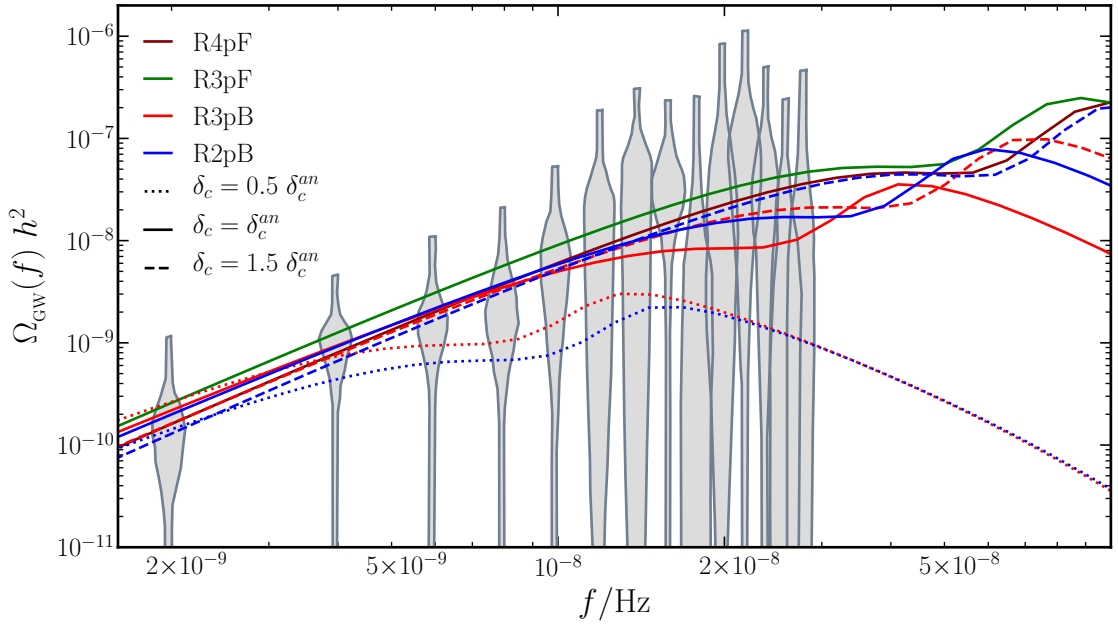


Figure 5. The spectral energy density of secondary GWs $\Omega_{\text{GW}}(f)$ that correspond to the best-fit values of the parameters in the four models, viz. R4pF, R3pF, R3pB and R2pB, are plotted. In the figure, we have also included the probability densities from the Kernel Density Estimators (KDEs) of the NANOGrav 15-year data (as gray violins) [223]. It is visually evident that, when $\delta_c = 0.5 \delta_c^{\text{an}}$, the spectral energy densities corresponding to the latter two models do not fit the data well.

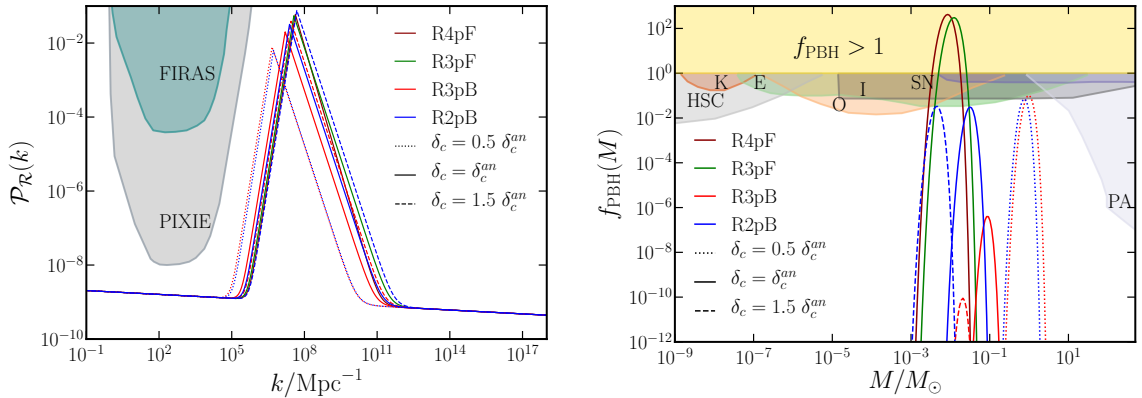


Figure 6. The inflationary scalar power spectrum $\mathcal{P}_{\mathcal{R}}(k)$ (on the left) and the fraction of PBHs that constitute the energy density of cold dark matter today $f_{\text{PBH}}(M)$ (on the right), which correspond to the best-fit values of the parameters in the four models are plotted. Clearly, in the case of the models R4pF and R3pF, the best-fit values lead to the overproduction of PBHs. It is also interesting to note that the best-fit inflationary scalar power spectra avoid the current and expected bounds from spectral distortions.

and the constraints on $f_{\text{PBH}}(M)$, respectively. Also, interestingly, we find that, in these

models, the higher the δ_c , the smaller is the value of M where the peaks of $f_{\text{PBH}}(M)$ occur. Lastly, from Fig. 6, it should also be clear that all the models are consistent with the current bounds on the primordial scalar power spectrum arrived at through the observations of the spectral distortions by FIRAS [224–226] or the future bounds expected from missions such as PIXIE [227, 228].

3.4 Primary GWs and constraints from ΔN_{eff}

We shall now turn to discuss the spectral energy density of primary GWs (i.e. the first-order tensor perturbations) that are generated during inflation from the quantum vacuum when no sources are present. Until now, there is no direct evidence of the primary GWs, but the CMB observations lead to an upper bound on their amplitude on large scales. The constraint on their strength is usually quoted in terms of the tensor-to-scalar ratio r , evaluated at or near the CMB pivot scale of $k_* \simeq 0.05 \text{ Mpc}^{-1}$. The latest CMB data from BICEP/Keck and Planck suggest that $r \lesssim 0.036$ [117].

Let γ_k^λ denote the Fourier modes associated with the first-order tensor perturbations. In the spatially flat FLRW universe, they satisfy the following equation of motion:

$$\gamma_k^{\lambda''} + 2aH\gamma_k^{\lambda'} + k^2\gamma_k^\lambda = 0, \quad (3.29)$$

which is essentially the same as the equation that describes the Fourier modes of the tensor perturbations at the second order [cf. Eq. (3.1)], but without a source. Consider a slow roll inflationary scenario driven by a single, canonical scalar field. In such a case, it is well known that the spectrum of primary GWs produced at the end of inflation proves to be nearly scale invariant, with an amplitude that is determined by the Hubble scale during inflation. The perturbations that are generated during inflation need to be evolved through the epochs of reheating and radiation domination, in order to arrive at the spectral energy density of primary GWs today (in this context, see, for example, Refs. [19, 229–246]). The strength and shape of the spectral density of primary GWs today are sensitive to the energy scale of inflation as well as the history of the background evolution after inflation.

For simplicity, let us consider inflation to be of the de Sitter form characterized by the constant Hubble parameter, say, H_1 ². In such a situation, as is well known, the scale of inflation can be expressed in terms of the tensor-to-scalar ratio r and the scalar amplitude A_s as follows: $H_1 = \pi M_{\text{Pl}} \sqrt{r A_s}/2$. Let us first focus on wave numbers that are significantly larger than the wave numbers associated with the CMB scales and which re-enter the Hubble radius during the epoch of radiation domination. After they enter the Hubble radius, the energy density associated with the GWs behave in the same manner as the energy density of radiation. Given a scale-invariant spectrum of primary GWs at the end of inflation, the dimensionless spectral energy density of primary GWs today, over wave numbers that re-enter the Hubble radius during radiation domination (i.e. over $k < k_{\text{re}}$) proves to be scale invariant as well, with an amplitude that is given by

$$\Omega_{\text{GW}}(k) h^2 = \Omega_r h^2 \frac{H_1^2}{12 \pi^2 M_{\text{Pl}}^2} = 3.5 \times 10^{-17} \left(\frac{H_1}{10^{-5} M_{\text{Pl}}} \right)^2, \quad (3.30)$$

²A priori, such an assumption may seem inconsistent with the inflationary model involving an epoch of ultra slow roll that is supposed to produce the scalar power spectrum (2.8). However, it is known that the de Sitter approximation for the scale factor works well during the epoch of ultra slow roll. Moreover, the departure from slow roll only leads to a step in an otherwise nearly scale-invariant tensor power spectrum (in this regard, see, for instance, Ref. [188], Fig. 3).

where $\Omega_r h^2 = 4.16 \times 10^{-5}$ denotes the present-day dimensionless energy density of radiation (i.e. including photons and all three species of neutrinos).

If there arises a phase of reheating between inflation and the epoch of radiation domination, then, evidently, the wave numbers over the range $k_{\text{re}} < k < k_e$ will re-enter the Hubble radius during the epoch of reheating. Needless to add, the wave number k_{re} depends on the EoS parameter w_{re} and the reheating temperature T_{re} . One finds that, over the wave numbers $k_{\text{re}} < k < k_e$, the spectral energy density of primary GWs today can be expressed as (see, for instance, Ref. [244] for detailed calculation)

$$\begin{aligned} \Omega_{\text{GW}}(k) h^2 &\simeq \Omega_r h^2 \frac{H_{\text{I}}^2}{12 \pi^2 M_{\text{Pl}}^2} \frac{\mu(w_{\text{re}})}{\pi} \left(\frac{k}{k_{\text{re}}} \right)^{n_{w_{\text{re}}}} \\ &\simeq 3.5 \times 10^{-17} \left(\frac{H_{\text{I}}}{10^{-5} M_{\text{Pl}}} \right)^2 \frac{\mu(w_{\text{re}})}{\pi} \left(\frac{k}{k_{\text{re}}} \right)^{n_{w_{\text{re}}}}, \end{aligned} \quad (3.31)$$

where the quantity $\mu(w_{\text{re}})$ and the index $n_{w_{\text{re}}}$ are given by

$$\mu(w_{\text{re}}) = (1 + 3 w_{\text{re}})^{4/(1+3 w_{\text{re}})} \Gamma^2 \left(\frac{5 + 3 w_{\text{re}}}{2 + 6 w_{\text{re}}} \right), \quad n_{w_{\text{re}}} = -\frac{2(1 - 3 w_{\text{re}})}{1 + 3 w_{\text{re}}}. \quad (3.32)$$

Note that, while $\mu(w_{\text{re}}) \simeq \mathcal{O}(1)$ for $0 \leq w_{\text{re}} \leq 1$, $n_{w_{\text{re}}}$ is positive or negative for $w_{\text{re}} > 1/3$ or $w_{\text{re}} < 1/3$, and vanishes $w_{\text{re}} = 1/3$. Moreover, the wave number k_e can be approximately expressed in terms of the inflationary energy scale H_{I} and the reheating parameters T_{re} and w_{re} as

$$k_e = a_e H_{\text{I}} \simeq H_{\text{I}} \frac{T_0}{T_{\text{re}}} \left(\frac{43}{11 g_{\text{s, re}}} \right)^{1/3} \left(\frac{\pi^2 g_{\text{re}} T_{\text{re}}^4}{90 M_{\text{Pl}}^2 H_{\text{I}}^2} \right)^{1/[3(1+w_{\text{re}})]}. \quad (3.33)$$

Since, at suitably late times (when the wave numbers of interest are inside the Hubble radius), the energy density of GWs behaves in the same manner as that of radiation, they can contribute additional relativistic degrees of freedom to radiation. These additional number of relativistic degrees of freedom, which is usually denoted as ΔN_{eff} , is well constrained by the CMB observations [9]. This constraint becomes particularly important when $w_{\text{re}} > 1/3$ because, in such cases, the spectral energy density of primary GWs has a positive spectral index for $k > k_{\text{re}}$. The constraint is given by (see, for instance, Refs. [19, 247])

$$\int_{k_{\text{re}}}^{k_e} \frac{dk}{k} \Omega_{\text{GW}}(k) h^2 \leq \frac{7}{8} \left(\frac{4}{11} \right)^{4/3} \Omega_{\gamma} h^2 \Delta N_{\text{eff}}, \quad (3.34)$$

where $\Omega_{\gamma} h^2 \simeq 2.47 \times 10^{-5}$ represents the energy density of photons today. Upon using the form (3.31) of $\Omega_{\text{GW}}(k)$, the above condition reduces to

$$\Omega_r h^2 \frac{H_{\text{I}}^2}{12 \pi^2 M_{\text{Pl}}^2} \frac{\mu(w_{\text{re}}) (1 + 3 w_{\text{re}})}{2 \pi (3 w_{\text{re}} - 1)} \left(\frac{k_e}{k_{\text{re}}} \right)^{\frac{6 w_{\text{re}} - 2}{1 + 3 w_{\text{re}}}} \leq 5.61 \times 10^{-6} \Delta N_{\text{eff}}. \quad (3.35)$$

Also, note that the ratio between k_e and k_{re} can be expressed as

$$\frac{k_e}{k_{\text{re}}} = \left(\frac{90 H_{\text{I}}^2 M_{\text{Pl}}^2}{\pi^2 g_{\text{re}}} \right)^{(1+3 w_{\text{re}})/[6(1+w_{\text{re}})]} T_{\text{re}}^{-2(1+3 w_{\text{re}})/[3(1+w_{\text{re}})]}. \quad (3.36)$$

Model	Maximum allowed value of r		
R4pF	0.036		
R3pF	0.036		
	$0.5 \delta_c^{\text{an}}$	δ_c^{an}	$1.5 \delta_c^{\text{an}}$
R3pB	4.2×10^{-8}	2.7×10^{-5}	0.036
R2pB	6.8×10^{-8}	2.4×10^{-3}	0.036

Table 3. We have listed the maximum allowed value of the tensor-to-scalar ratio r that is consistent with the reheating temperature of $T_{\text{re}} = 50$ MeV, the best-fit values of w_{re} arrived at on comparison with the NANOGrav 15-year data [cf. Tab. 1], and the constraint $\Delta N_{\text{eff}} < 0.284$ from Planck [9]. We have listed the values of r for the four models we discussed earlier, viz. R4pF, R3pF, R3pB and R2pB.

The above three equations can then be combined to arrive at the following bound on the reheating temperature T_{re} :

$$T_{\text{re}} \geq \left[\frac{\Omega_{\text{r}} h^2}{5.61 \times 10^{-6} \Delta N_{\text{eff}}} \frac{H_1^2}{12 \pi^2 M_{\text{Pl}}^2} \frac{\mu(w_{\text{re}}) (1 + 3 w_{\text{re}})}{2 \pi (3 w_{\text{re}} - 1)} \right]^{\frac{3(1+w_{\text{re}})}{4(3w_{\text{re}}-1)}} \left(\frac{90 H_1^2 M_{\text{Pl}}^2}{\pi^2 g_{\text{re}}} \right)^{\frac{1}{4}}. \quad (3.37)$$

This condition implies that, for a given $(T_{\text{re}}, w_{\text{re}})$, the bound on ΔN_{eff} leads to a restriction on the energy scale of inflation H_1 or, equivalently, on the tensor-to-scalar ratio r [248]. Recall that, in our comparison of secondary GWs with the NANOGrav 15-year data in the previous section, we had fixed the reheating temperature to be $T_{\text{re}} = 50$ MeV, just above the standard BBN value of about 4 MeV. Given T_{re} , the best-fit values of w_{re} from Tab. 1 and the CMB constraint $\Delta N_{\text{eff}} < 0.284$ [9], we can calculate the value of the tensor-to-scalar ratio r that is consistent with the bound (3.37) above. In Tab. 3, we have listed these maximum allowed values of r , for the four models we have considered earlier, viz. R4pF, R3pF, R3pB and R2pB. In Fig. 2, we have plotted the dimensionless spectral density of primary GWs today corresponding to $r = 0.036$, $T_{\text{re}} = 50$ MeV and values of w_{re} for which we had plotted the spectral density of secondary GWs generated due to excess scalar power on small scales. We have plotted the primary spectral energy densities until the frequencies that correspond to k_e for each of the parameters, which is determined by the relation (3.33).

4 Conclusions and discussion

Significant amounts of PBHs can be formed in scenarios wherein the inflationary scalar power spectrum is considerably amplified on small scales when compared to the COBE normalized values on the CMB scales. In such situations, as the PBHs are formed when the wave numbers re-enter the Hubble radius either during the phase of reheating or during the epoch of radiation domination, secondary GWs of considerable strengths are inevitably induced by the excess scalar power on small scales. In this work, we examined whether the secondary GWs generated in such a scenario can explain the NANOGrav 15-year data, without the overproduction of solar mass PBHs, an issue that has been plaguing some of the recent analyses in this context. We have listed below the main conclusions of our analysis.

- To begin with, as one would have expected, we find that an extended phase of reheating affects the abundance of PBHs as well as the spectral energy densities of both the primary

and secondary GWs. For a given primordial scalar power spectrum, the parameters describing reheating, viz. T_{re} and w_{re} , not only influence the masses of the PBHs formed, but they also affect the number of PBHs produced over the corresponding mass range. In Fig. 1, we illustrated the dependence of $f_{\text{PBH}}(M)$ on the parameters k_{peak} , T_{re} and w_{re} , assuming fixed values for A_0 and n_0 . We find that, for fixed values of T_{re} and w_{re} , as we increase k_{peak} , the maximum value of $f_{\text{PBH}}(M)$ behaves as $M^{-2w_{\text{re}}/(1+w_{\text{re}})}$. Moreover, for given k_{peak} and w_{re} , as T_{re} changes, the maximum value of $f_{\text{PBH}}(M)$ varies as M when $w_{\text{re}} < 1/3$ and as M^{-1} when $w_{\text{re}} > 1/3$. However, when w_{re} is varied with the other two parameters fixed, the behavior of the maximum value of $f_{\text{PBH}}(M)$ is not linear. For a given k_{peak} and T_{re} , the maximum of $f_{\text{PBH}}(M)$ has the lowest value when $w_{\text{re}} = 1/3$ and it increases on either side as we move away from w_{re} of $1/3$.

- Secondly, to address the issue of overproduction of PBHs as one attempts to explain the NANOGrav 15-year data in terms of the secondary GWs generated due to enhanced scalar power on small scales, we carried out MCMC runs without and with the constraints on $f_{\text{PBH}}(M)$. We find that, if we do not include the bounds on $f_{\text{PBH}}(M)$ (as in the case of the models R4pF and R3pF), the best-fit values arrived at upon comparing the models with the NANOGrav 15-year data indeed leads to the formation of excessive number of PBHs [with $f_{\text{PBH}}(M) > 1$]. In order to circumvent this difficulty, we carried out MCMC runs which ensure that either $f_{\text{PBH}}(M) < 1$ (as in the case of the model R3pB) or remain consistent with the available observational bounds on $f_{\text{PBH}}(M)$ (as in the model R2pB). These points should be evident from Fig. 5 wherein we have plotted $f_{\text{PBH}}(M)$ for the best-fit values (listed in Tab.1) of the four models. Importantly, we find that, if we consider the formation of PBHs during a prolonged phase of reheating with the EoS parameter lying in the range of 0.5–0.65, then, it is possible to remain within the maximum allowed abundance of PBHs and simultaneously account for the NANOGrav 15-year data with a very strong Bayesian preference (as should be clear from Tab. 2), when compared to the astrophysical model of SMBHBs.
- Thirdly, in our analysis, we also accounted for the impact of the uncertainties in the collapse condition, in particular, the value of the critical density δ_c , on the formation of PBHs. As one can intuitively predict, assuming a lower value of δ_c can lead to an acute overproduction of PBHs, whereas a higher value of δ_c can significantly suppress the number of PBHs formed, thereby allowing a larger volume of the parameter space to be compatible with the SGWB suggested by the NANOGrav 15-year data. This is clearly reflected in the Bayesian factor (listed in Tab. 2) for the model R2pB. Note that the Bayesian factor is considerably higher when $\delta_c = 1.5 \delta_c^{\text{an}}$ than when $\delta_c = 0.5 \delta_c^{\text{an}}$.
- Lastly, since the spectral density of primary GWs has a blue tilt for $w_{\text{re}} > 1/3$, it can lead to a violation of the constraint on the number of relativistic degrees of freedom during BBN. We take into account the latest constraints on ΔN_{eff} to arrive at bounds on the tensor-to-scalar ratio r for the best-fit values of the parameter w_{re} (see Tab. 3). Interestingly, we find that, in the models R3pB and R2pB, the constraint on r from ΔN_{eff} proves to be more stringent than the bound from the CMB observations [117].

In this work, we have remained agnostic about the origin of the primordial scalar power spectrum. We have assumed a broken power law form for the spectrum, without specifying an inflationary model to generate it. The form of the spectrum has been motivated by the typical spectra that arise in single field models of inflation which permit a brief epoch of

ultra slow roll. Needless to add, it will be worthwhile to extend our analysis and investigate particular inflationary models that generate such spectra. As non-Gaussianities are expected to be relatively large in scenarios involving ultra slow roll inflation [188], constructing such a model will not only allow us to explicitly evaluate the non-Gaussianities generated in these models, but also study their effects on the generation of both PBHs [249–251] and secondary GWs [252]. Another important aspect that we need to take into account is the effects due to a gradual transition from the phase of reheating to the epoch of radiation domination. In order to consider these effects, we will first need to develop theoretical as well as numerical frameworks to study the formation of PBHs in backgrounds with a time-dependent EoS parameter. With the necessary tools at hand, we can study the possibility of such scenarios to be able to explain the PTA data satisfactorily. We are presently working on some of these issues.

Acknowledgements

SM and LS wish to thank the Indian Institute of Technology Madras, Chennai, India, for support through the Exploratory Research Project RF22230527PHRFER008479. NB wishes to thank his parents for their selfless support that never ceased during this work or any of NB’s earlier works. During this work, NB was supported by the institute postdoctoral fellowship (IPDF) of the Indian Institute of Technology Madras, Chennai, India, and later by postdoctoral fellowship of International Centre for Theoretical Physics Asia-Pacific (ICTP-AP), Beijing, China. NB also thanks Rajeev Kumar Jain and Ranjan Laha for the initial collaborations and fruitful discussions on the generation of scalar-induced SGWB during the phase of reheating, specifically in the context of the resonant amplification of the SGWB. MRH wishes to acknowledge support from the Science and Engineering Research Board (SERB), Department of Science and Technology (DST), Government of India (GoI), through the National Postdoctoral Fellowship PDF/2022/002988. DM and LS gratefully acknowledge the support received from SERB, DST, GoI, through the Core Research Grant CRG/2020/003664. LS also wishes to thank the Indo-French Centre for the Promotion of Advanced Research for support of the proposal 6704-4 under the Collaborative Scientific Research Programme. We also thank our referee in JCAP for his/her fruitful comments, which helped us improve the discussions in the manuscript. During this work, NB was supported by the institute postdoctoral fellowship (IPDF) of the Indian Institute of Technology Madras, Chennai, India, and later by postdoctoral fellowship of International Centre for Theoretical Physics Asia-Pacific (ICTP-AP), Beijing, China.

Note added

During the completion of this work, a preprint appeared on the arXiv [137], which also studies the generation of secondary GWs during reheating, induced by primordial scalar power spectra that contain either a delta function or a lognormal peak on small scales. The work also compares the spectral density of GWs with the NANOGrav data. In the models R4pF and R3pF, we have also considered primordial scalar spectra with enhanced power on small scales, but in the form of a broken power law. To ensure that the optimal parameters do not lead to the overproduction of PBHs, in our work, we have further carried out runs which *simultaneously* calculate $f_{\text{PBH}}(M)$ and scan the parameter space that is restricted to either $f_{\text{PBH}} < 1$ (in the model referred to as R3pB) or is consistent with the available mass-dependent

constraints on $f_{\text{PBH}}(M)$ (in the model R2pB). Moreover, in the models R3pB and R2pB, we have explicitly accounted for the uncertainty in δ_c . Further, in the case of the model R2pB, using the **enterprise** mode of PTArcade, we have evaluated the Bayesian evidences associated with the optimal scenarios for different values of δ_c . We have also considered the primary GWs generated in the scenario and discussed the impact of the constraints from ΔN_{eff} on the tensor-to-scalar ratio or, equivalently, the energy scale of inflation.

References

- [1] C. L. Bennett, A. Banday, K. M. Gorski, G. Hinshaw, P. Jackson, P. Keegstra, A. Kogut, G. F. Smoot, D. T. Wilkinson, and E. L. Wright, *Four year COBE DMR cosmic microwave background observations: Maps and basic results*, *Astrophys. J. Lett.* **464** (1996) L1–L4, [[astro-ph/9601067](#)].
- [2] G. F. Smoot, *COBE observations and results*, *AIP Conf. Proc.* **476** (1999), no. 1 1–10, [[astro-ph/9902027](#)].
- [3] **WMAP** Collaboration, E. Komatsu et al., *Five-Year Wilkinson Microwave Anisotropy Probe (WMAP) Observations: Cosmological Interpretation*, *Astrophys. J. Suppl.* **180** (2009) 330–376, [[arXiv:0803.0547](#)].
- [4] **WMAP** Collaboration, E. Komatsu et al., *Seven-Year Wilkinson Microwave Anisotropy Probe (WMAP) Observations: Cosmological Interpretation*, *Astrophys. J. Suppl.* **192** (2011) 18, [[arXiv:1001.4538](#)].
- [5] **WMAP** Collaboration, G. Hinshaw et al., *Nine-Year Wilkinson Microwave Anisotropy Probe (WMAP) Observations: Cosmological Parameter Results*, *Astrophys. J. Suppl.* **208** (2013) 19, [[arXiv:1212.5226](#)].
- [6] **WMAP** Collaboration, C. L. Bennett et al., *Nine-Year Wilkinson Microwave Anisotropy Probe (WMAP) Observations: Final Maps and Results*, *Astrophys. J. Suppl.* **208** (2013) 20, [[arXiv:1212.5225](#)].
- [7] **Planck** Collaboration, P. A. R. Ade et al., *Planck 2013 results. XVI. Cosmological parameters*, *Astron. Astrophys.* **571** (2014) A16, [[arXiv:1303.5076](#)].
- [8] **Planck** Collaboration, P. A. R. Ade et al., *Planck 2015 results. XIII. Cosmological parameters*, *Astron. Astrophys.* **594** (2016) A13, [[arXiv:1502.01589](#)].
- [9] **Planck** Collaboration, N. Aghanim et al., *Planck 2018 results. VI. Cosmological parameters*, *Astron. Astrophys.* **641** (2020) A6, [[arXiv:1807.06209](#)]. [Erratum: *Astron. Astrophys.* 652, C4 (2021)].
- [10] **Planck** Collaboration, Y. Akrami et al., *Planck 2018 results. X. Constraints on inflation*, *Astron. Astrophys.* **641** (2020) A10, [[arXiv:1807.06211](#)].
- [11] **Planck** Collaboration, Y. Akrami et al., *Planck 2018 results. IX. Constraints on primordial non-Gaussianity*, *Astron. Astrophys.* **641** (2020) A9, [[arXiv:1905.05697](#)].
- [12] **LIGO Scientific, Virgo** Collaboration, B. P. Abbott et al., *Observation of Gravitational Waves from a Binary Black Hole Merger*, *Phys. Rev. Lett.* **116** (2016), no. 6 061102, [[arXiv:1602.03837](#)].
- [13] **LIGO Scientific, Virgo** Collaboration, B. P. Abbott et al., *Binary Black Hole Mergers in the first Advanced LIGO Observing Run*, *Phys. Rev. X* **6** (2016), no. 4 041015, [[arXiv:1606.04856](#)]. [Erratum: *Phys. Rev. X* 8, 039903 (2018)].
- [14] **LIGO Scientific, Virgo** Collaboration, B. P. Abbott et al., *The basic physics of the binary black hole merger GW150914*, *Annalen Phys.* **529** (2017), no. 1-2 1600209, [[arXiv:1608.01940](#)].

- [15] **LIGO Scientific, VIRGO** Collaboration, B. P. Abbott et al., *GW170104: Observation of a 50-Solar-Mass Binary Black Hole Coalescence at Redshift 0.2*, *Phys. Rev. Lett.* **118** (2017), no. 22 221101, [[arXiv:1706.01812](#)]. [Erratum: *Phys.Rev.Lett.* 121, 129901 (2018)].
- [16] **LIGO Scientific, Virgo** Collaboration, B. P. Abbott et al., *GW170814: A Three-Detector Observation of Gravitational Waves from a Binary Black Hole Coalescence*, *Phys. Rev. Lett.* **119** (2017), no. 14 141101, [[arXiv:1709.09660](#)].
- [17] **LIGO Scientific, Virgo** Collaboration, B. . P. . Abbott et al., *GW170608: Observation of a 19-solar-mass Binary Black Hole Coalescence*, *Astrophys. J. Lett.* **851** (2017) L35, [[arXiv:1711.05578](#)].
- [18] M. C. Guzzetti, N. Bartolo, M. Liguori, and S. Matarrese, *Gravitational waves from inflation*, *Riv. Nuovo Cim.* **39** (2016), no. 9 399–495, [[arXiv:1605.01615](#)].
- [19] C. Caprini and D. G. Figueroa, *Cosmological Backgrounds of Gravitational Waves*, *Class. Quant. Grav.* **35** (2018), no. 16 163001, [[arXiv:1801.04268](#)].
- [20] G. Domènech, *Scalar Induced Gravitational Waves Review*, *Universe* **7** (2021), no. 11 398, [[arXiv:2109.01398](#)].
- [21] R. Roshan and G. White, *Using gravitational waves to see the first second of the Universe*, [arXiv:2401.04388](#).
- [22] **KAGRA, Virgo, LIGO Scientific** Collaboration, R. Abbott et al., *Upper limits on the isotropic gravitational-wave background from Advanced LIGO and Advanced Virgo’s third observing run*, *Phys. Rev. D* **104** (2021), no. 2 022004, [[arXiv:2101.12130](#)].
- [23] **NANOGrav** Collaboration, G. Agazie et al., *The NANOGrav 15-year Data Set: Evidence for a Gravitational-Wave Background*, [arXiv:2306.16213](#).
- [24] **NANOGrav** Collaboration, G. Agazie et al., *The NANOGrav 15-year Data Set: Observations and Timing of 68 Millisecond Pulsars*, [arXiv:2306.16217](#).
- [25] **European Pulsar Timing Array Collaboration** Collaboration, J. Antoniadis et al., *The second data release from the European Pulsar Timing Array I. The dataset and timing analysis*, [arXiv:2306.16224](#).
- [26] **EPTA** Collaboration, J. Antoniadis et al., *The second data release from the European Pulsar Timing Array III. Search for gravitational wave signals*, [arXiv:2306.16214](#).
- [27] **Parkes Pulsar Timing Array Collaboration** Collaboration, A. Zic et al., *The Parkes Pulsar Timing Array Third Data Release*, [arXiv:2306.16230](#).
- [28] **Parkes Pulsar Timing Array Collaboration** Collaboration, D. J. Reardon et al., *Search for an isotropic gravitational-wave background with the Parkes Pulsar Timing Array*, [arXiv:2306.16215](#).
- [29] **Chinese Pulsar Timing Array Collaboration** Collaboration, H. Xu et al., *Searching for the nano-Hertz stochastic gravitational wave background with the Chinese Pulsar Timing Array Data Release I*, [arXiv:2306.16216](#).
- [30] **NANOGrav** Collaboration, A. Afzal et al., *The NANOGrav 15-year Data Set: Search for Signals from New Physics*, [arXiv:2306.16219](#).
- [31] K. Inomata, K. Kohri, and T. Terada, *The Detected Stochastic Gravitational Waves and Subsolar-Mass Primordial Black Holes*, [arXiv:2306.17834](#).
- [32] G. Franciolini, A. Iovino, Junior., V. Vaskonen, and H. Veermae, *The recent gravitational wave observation by pulsar timing arrays and primordial black holes: the importance of non-gaussianities*, [arXiv:2306.17149](#).
- [33] K. Cheung, C. J. Ouseph, and P.-Y. Tseng, *NANOGrav Signal and PBH from the Modified Higgs Inflation*, [arXiv:2307.08046](#).

- [34] S. Balaji, G. Domènech, and G. Franciolini, *Scalar-induced gravitational wave interpretation of PTA data: the role of scalar fluctuation propagation speed*, [arXiv:2307.08552](#).
- [35] H. Firouzjahi and A. Talebian, *Induced Gravitational Waves from Ultra Slow-Roll Inflation and Pulsar Timing Arrays Observations*, [arXiv:2307.03164](#).
- [36] C. Unal, A. Papageorgiou, and I. Obata, *Axion-Gauge Dynamics During Inflation as the Origin of Pulsar Timing Array Signals and Primordial Black Holes*, [arXiv:2307.02322](#).
- [37] L. Frosina and A. Urbano, *On the inflationary interpretation of the nHz gravitational-wave background*, [arXiv:2308.06915](#).
- [38] L. Liu, Z.-C. Chen, and Q.-G. Huang, *Implications for the non-Gaussianity of curvature perturbation from pulsar timing arrays*, [arXiv:2307.01102](#).
- [39] S. A. Hosseini Mansoori, F. Felegray, A. Talebian, and M. Sami, *PBHs and GWs from T^2 -inflation and NANOGrav 15-year data*, [arXiv:2307.06757](#).
- [40] L. Liu, Z.-C. Chen, and Q.-G. Huang, *Probing the equation of state of the early Universe with pulsar timing arrays*, [arXiv:2307.14911](#).
- [41] N. Bhaumik, R. K. Jain, and M. Lewicki, *Ultralow mass primordial black holes in the early Universe can explain the pulsar timing array signal*, *Phys. Rev. D* **108** (2023), no. 12 123532, [[arXiv:2308.07912](#)].
- [42] P. F. Depta, K. Schmidt-Hoberg, and C. Tasillo, *Do pulsar timing arrays observe merging primordial black holes?*, [arXiv:2306.17836](#).
- [43] Y. Gouttenoire, S. Trifinopoulos, G. Valogiannis, and M. Vanvlasselaer, *Scrutinizing the Primordial Black Holes Interpretation of PTA Gravitational Waves and JWST Early Galaxies*, [arXiv:2307.01457](#).
- [44] A. Salvio, *Supercooling in Radiative Symmetry Breaking: Theory Extensions, Gravitational Wave Detection and Primordial Black Holes*, [arXiv:2307.04694](#).
- [45] Y. Gouttenoire, *First-order Phase Transition interpretation of PTA signal produces solar-mass Black Holes*, [arXiv:2307.04239](#).
- [46] T. Ghosh, A. Ghoshal, H.-K. Guo, F. Hajkarim, S. F. King, K. Sinha, X. Wang, and G. White, *Did we hear the sound of the Universe boiling? Analysis using the full fluid velocity profiles and NANOGrav 15-year data*, [arXiv:2307.02259](#).
- [47] H. An, B. Su, H. Tai, L.-T. Wang, and C. Yang, *Phase transition during inflation and the gravitational wave signal at pulsar timing arrays*, [arXiv:2308.00070](#).
- [48] S. Jiang, A. Yang, J. Ma, and F. P. Huang, *Implication of nano-Hertz stochastic gravitational wave on dynamical dark matter through a first-order phase transition*, [arXiv:2306.17827](#).
- [49] P. Athron, A. Fowlie, C.-T. Lu, L. Morris, L. Wu, Y. Wu, and Z. Xu, *Can supercooled phase transitions explain the gravitational wave background observed by pulsar timing arrays?*, [arXiv:2306.17239](#).
- [50] P. Di Bari and M. H. Rahat, *The split majoron model confronts the NANOGrav signal*, [arXiv:2307.03184](#).
- [51] S.-P. Li and K.-P. Xie, *A collider test of nano-Hertz gravitational waves from pulsar timing arrays*, [arXiv:2307.01086](#).
- [52] J. Ellis, M. Lewicki, C. Lin, and V. Vaskonen, *Cosmic Superstrings Revisited in Light of NANOGrav 15-Year Data*, [arXiv:2306.17147](#).
- [53] G. Lazarides, R. Maji, and Q. Shafi, *Superheavy quasi-stable strings and walls bounded by strings in the light of NANOGrav 15 year data*, [arXiv:2306.17788](#).
- [54] Z. Zhang, C. Cai, Y.-H. Su, S. Wang, Z.-H. Yu, and H.-H. Zhang, *Nano-Hertz gravitational*

waves from collapsing domain walls associated with freeze-in dark matter in light of pulsar timing array observations, [arXiv:2307.11495](#).

- [55] M. Yamada and K. Yonekura, *Dark baryon from pure Yang-Mills theory and its GW signature from cosmic strings*, [arXiv:2307.06586](#).
- [56] B.-Q. Lu and C.-W. Chiang, *Nano-Hertz stochastic gravitational wave background from domain wall annihilation*, [arXiv:2307.00746](#).
- [57] E. Babichev, D. Gorbunov, S. Ramazanov, R. Samanta, and A. Vikman, *NANOGrav spectral index $\gamma = 3$ from melting domain walls*, [arXiv:2307.04582](#).
- [58] S. Ge, *Stochastic gravitational wave background: birth from axionic string-wall death*, [arXiv:2307.08185](#).
- [59] X.-F. Li, *Probing the high temperature symmetry breaking with gravitational waves from domain walls*, [arXiv:2307.03163](#).
- [60] N. Kitajima, J. Lee, K. Murai, F. Takahashi, and W. Yin, *Nanohertz Gravitational Waves from Axion Domain Walls Coupled to QCD*, [arXiv:2306.17146](#).
- [61] S. F. King, D. Marfatia, and M. H. Rahat, *Towards distinguishing Dirac from Majorana neutrino mass with gravitational waves*, [arXiv:2306.05389](#).
- [62] G. Lazarides, R. Maji, A. Moursy, and Q. Shafi, *Inflation, superheavy metastable strings and gravitational waves in non-supersymmetric flipped $SU(5)$* , [arXiv:2308.07094](#).
- [63] X. Niu and M. H. Rahat, *NANOGrav signal from axion inflation*, [arXiv:2307.01192](#).
- [64] K. Murai and W. Yin, *A Novel Probe of Supersymmetry in Light of Nanohertz Gravitational Waves*, [arXiv:2307.00628](#).
- [65] S. Vagnozzi, *Inflationary interpretation of the stochastic gravitational wave background signal detected by pulsar timing array experiments*, *JHEAp* **39** (2023) 81–98, [[arXiv:2306.16912](#)].
- [66] D. Borah, S. Jyoti Das, and R. Samanta, *Imprint of inflationary gravitational waves and WIMP dark matter in pulsar timing array data*, *JCAP* **03** (2024) 031, [[arXiv:2307.00537](#)].
- [67] S. Datta, *Inflationary gravitational waves, pulsar timing data and low-scale-leptogenesis*, [arXiv:2307.00646](#).
- [68] S. Choudhury, *Single field inflation in the light of NANOGrav 15-year Data: Quintessential interpretation of blue tilted tensor spectrum through Non-Bunch Davies initial condition*, [arXiv:2307.03249](#).
- [69] S. Maiti, D. Maity, and L. Sriramkumar, *Constraining inflationary magnetogenesis and reheating via GWs in light of PTA data*, [arXiv:2401.01864](#).
- [70] G. Ye and A. Silvestri, *Can the Gravitational Wave Background Feel Wiggles in Spacetime?*, *Astrophys. J. Lett.* **963** (2024), no. 1 L15, [[arXiv:2307.05455](#)].
- [71] Z.-C. Chen and L. Liu, *Can we distinguish the adiabatic fluctuations and isocurvature fluctuations with pulsar timing arrays?*, [arXiv:2402.16781](#).
- [72] M. R. Gangopadhyay, V. V. Godithi, K. Ichiki, R. Inui, T. Kajino, A. Manusankar, G. J. Mathews, and Yogesh, *Is the NANOGrav detection evidence of resonant particle creation during inflation?*, [arXiv:2309.03101](#).
- [73] S. Hawking, *Gravitationally collapsed objects of very low mass*, *Mon. Not. Roy. Astron. Soc.* **152** (1971) 75.
- [74] B. J. Carr and S. W. Hawking, *Black Holes in the Early Universe*, *Monthly Notices of the Royal Astronomical Society* **168** (08, 1974) 399–415, [<https://academic.oup.com/mnras/article-pdf/168/2/399/8079885/mnras168-0399.pdf>].

- [75] B. Carr and F. Kuhnel, *Primordial Black Holes as Dark Matter: Recent Developments*, *Ann. Rev. Nucl. Part. Sci.* **70** (2020) 355–394, [[arXiv:2006.02838](#)].
- [76] B. Carr and F. Kuhnel, *Primordial black holes as dark matter candidates*, *SciPost Phys. Lect. Notes* **48** (2022) 1, [[arXiv:2110.02821](#)].
- [77] P. Montero-Camacho, X. Fang, G. Vasquez, M. Silva, and C. M. Hirata, *Revisiting constraints on asteroid-mass primordial black holes as dark matter candidates*, *JCAP* **08** (2019) 031, [[arXiv:1906.05950](#)].
- [78] S. W. Hawking, I. G. Moss, and J. M. Stewart, *Bubble Collisions in the Very Early Universe*, *Phys. Rev. D* **26** (1982) 2681.
- [79] G. Scelfo, N. Bellomo, A. Raccanelli, S. Matarrese, and L. Verde, *GW×LSS: chasing the progenitors of merging binary black holes*, *JCAP* **09** (2018) 039, [[arXiv:1809.03528](#)].
- [80] I. G. Moss, *Singularity formation from colliding bubbles*, *Phys. Rev. D* **50** (Jul, 1994) 676–681.
- [81] S. G. Rubin, A. S. Sakharov, and M. Y. Khlopov, *The Formation of primary galactic nuclei during phase transitions in the early universe*, *J. Exp. Theor. Phys.* **91** (2001) 921–929, [[hep-ph/0106187](#)].
- [82] V. Dokuchaev, Y. Eroshenko, and S. Rubin, *Quasars formation around clusters of primordial black holes*, *Grav. Cosmol.* **11** (2005) 99–104, [[astro-ph/0412418](#)].
- [83] J. Garriga, A. Vilenkin, and J. Zhang, *Black holes and the multiverse*, *JCAP* **02** (2016) 064, [[arXiv:1512.01819](#)].
- [84] H. Deng, J. Garriga, and A. Vilenkin, *Primordial black hole and wormhole formation by domain walls*, *JCAP* **04** (2017) 050, [[arXiv:1612.03753](#)].
- [85] S. Ge, *Sublunar-Mass Primordial Black Holes from Closed Axion Domain Walls*, *Phys. Dark Univ.* **27** (2020) 100440, [[arXiv:1905.12182](#)].
- [86] J. Liu, Z.-K. Guo, and R.-G. Cai, *Primordial Black Holes from Cosmic Domain Walls*, *Phys. Rev. D* **101** (2020), no. 2 023513, [[arXiv:1908.02662](#)].
- [87] C. J. Hogan, *Massive black holes generated by cosmic strings*, *Physics Letters B* **143** (1984), no. 1 87–91.
- [88] S. Hawking, *Black holes from cosmic strings*, *Physics Letters B* **231** (1989), no. 3 237–239.
- [89] A. Polnarev and R. Zembowicz, *Formation of primordial black holes by cosmic strings*, *Phys. Rev. D* **43** (Feb, 1991) 1106–1109.
- [90] J. H. MacGibbon, R. H. Brandenberger, and U. F. Wichoski, *Limits on black hole formation from cosmic string loops*, *Phys. Rev. D* **57** (1998) 2158–2165, [[astro-ph/9707146](#)].
- [91] **Planck** Collaboration, P. A. R. Ade et al., *Planck 2013 results. XXV. Searches for cosmic strings and other topological defects*, *Astron. Astrophys.* **571** (2014) A25, [[arXiv:1303.5085](#)].
- [92] J. J. Blanco-Pillado, K. D. Olum, and X. Siemens, *New limits on cosmic strings from gravitational wave observation*, *Phys. Lett. B* **778** (2018) 392–396, [[arXiv:1709.02434](#)].
- [93] S. J. Huber, T. Konstandin, G. Nardini, and I. Rues, *Detectable Gravitational Waves from Very Strong Phase Transitions in the General NMSSM*, *JCAP* **03** (2016) 036, [[arXiv:1512.06357](#)].
- [94] C. Caprini et al., *Science with the space-based interferometer eLISA. II: Gravitational waves from cosmological phase transitions*, *JCAP* **04** (2016) 001, [[arXiv:1512.06239](#)].
- [95] P. S. B. Dev and A. Mazumdar, *Probing the Scale of New Physics by Advanced LIGO/VIRGO*, *Phys. Rev. D* **93** (2016), no. 10 104001, [[arXiv:1602.04203](#)].
- [96] D. G. Figueroa, M. Hindmarsh, and J. Urrestilla, *Exact Scale-Invariant Background of Gravitational Waves from Cosmic Defects*, *Phys. Rev. Lett.* **110** (2013), no. 10 101302,

- [arXiv:1212.5458].
- [97] S. A. Sanidas, R. A. Battye, and B. W. Stappers, *Constraints on cosmic string tension imposed by the limit on the stochastic gravitational wave background from the European Pulsar Timing Array*, *Phys. Rev. D* **85** (2012) 122003, [arXiv:1201.2419].
- [98] P. Ivanov, P. Naselsky, and I. Novikov, *Inflation and primordial black holes as dark matter*, *Phys. Rev. D* **50** (Dec, 1994) 7173–7178.
- [99] J. Yokoyama, *Chaotic new inflation and formation of primordial black holes*, *Phys. Rev. D* **58** (1998) 083510, [astro-ph/9802357].
- [100] W. H. Kinney, *Horizon crossing and inflation with large eta*, *Phys. Rev. D* **72** (2005) 023515, [gr-qc/0503017].
- [101] K. Kohri, D. H. Lyth, and A. Melchiorri, *Black hole formation and slow-roll inflation*, *JCAP* **04** (2008) 038, [arXiv:0711.5006].
- [102] L. Alabidi and K. Kohri, *Generating Primordial Black Holes Via Hilltop-Type Inflation Models*, *Phys. Rev. D* **80** (2009) 063511, [arXiv:0906.1398].
- [103] J. Garcia-Bellido and E. Ruiz Morales, *Primordial black holes from single field models of inflation*, *Phys. Dark Univ.* **18** (2017) 47–54, [arXiv:1702.03901].
- [104] C. Pattison, V. Vennin, H. Assadullahi, and D. Wands, *Quantum diffusion during inflation and primordial black holes*, *JCAP* **10** (2017) 046, [arXiv:1707.00537].
- [105] G. Ballesteros and M. Taoso, *Primordial black hole dark matter from single field inflation*, *Phys. Rev. D* **97** (2018), no. 2 023501, [arXiv:1709.05565].
- [106] M. P. Hertzberg and M. Yamada, *Primordial Black Holes from Polynomial Potentials in Single Field Inflation*, *Phys. Rev. D* **97** (2018), no. 8 083509, [arXiv:1712.09750].
- [107] M. Biagetti, G. Franciolini, A. Kehagias, and A. Riotto, *Primordial Black Holes from Inflation and Quantum Diffusion*, *JCAP* **07** (2018) 032, [arXiv:1804.07124].
- [108] J. M. Ezquiaga and J. García-Bellido, *Quantum diffusion beyond slow-roll: implications for primordial black-hole production*, *JCAP* **08** (2018) 018, [arXiv:1805.06731].
- [109] J. Martin, *Inflation and precision cosmology*, *Braz. J. Phys.* **34** (2004) 1307–1321, [astro-ph/0312492].
- [110] J. Martin, *Inflationary cosmological perturbations of quantum-mechanical origin*, *Lect. Notes Phys.* **669** (2005) 199–244, [hep-th/0406011].
- [111] B. A. Bassett, S. Tsujikawa, and D. Wands, *Inflation dynamics and reheating*, *Rev. Mod. Phys.* **78** (2006) 537–589, [astro-ph/0507632].
- [112] L. Sriramkumar, *An introduction to inflation and cosmological perturbation theory*, arXiv:0904.4584.
- [113] D. Baumann and H. V. Peiris, *Cosmological Inflation: Theory and Observations*, *Adv. Sci. Lett.* **2** (2009) 105–120, [arXiv:0810.3022].
- [114] L. Sriramkumar, *On the generation and evolution of perturbations during inflation and reheating*, pp. 207–249. 2012.
- [115] J. Martin, *The Observational Status of Cosmic Inflation after Planck*, *Astrophys. Space Sci. Proc.* **45** (2016) 41–134, [arXiv:1502.05733].
- [116] **Planck** Collaboration, P. A. R. Ade et al., *Planck 2015 results. XX. Constraints on inflation*, *Astron. Astrophys.* **594** (2016) A20, [arXiv:1502.02114].
- [117] **BICEP, Keck** Collaboration, P. A. R. Ade et al., *Improved Constraints on Primordial Gravitational Waves using Planck, WMAP, and BICEP/Keck Observations through the 2018*

- Observing Season*, *Phys. Rev. Lett.* **127** (2021), no. 15 151301, [[arXiv:2110.00483](#)].
- [118] N. C. Tsamis and R. P. Woodard, *Improved estimates of cosmological perturbations*, *Phys. Rev. D* **69** (2004) 084005, [[astro-ph/0307463](#)].
- [119] C. Germani and T. Prokopec, *On primordial black holes from an inflection point*, *Phys. Dark Univ.* **18** (2017) 6–10, [[arXiv:1706.04226](#)].
- [120] J. M. Ezquiaga, J. Garcia-Bellido, and E. Ruiz Morales, *Primordial Black Hole production in Critical Higgs Inflation*, *Phys. Lett. B* **776** (2018) 345–349, [[arXiv:1705.04861](#)].
- [121] I. Dalianis, A. Kehagias, and G. Tringas, *Primordial black holes from α -attractors*, *JCAP* **01** (2019) 037, [[arXiv:1805.09483](#)].
- [122] N. Bhaumik and R. K. Jain, *Primordial black holes dark matter from inflection point models of inflation and the effects of reheating*, *JCAP* **01** (2020) 037, [[arXiv:1907.04125](#)].
- [123] H. V. Ragavendra, P. Saha, L. Sriramkumar, and J. Silk, *Primordial black holes and secondary gravitational waves from ultraslow roll and punctuated inflation*, *Phys. Rev. D* **103** (2021), no. 8 083510, [[arXiv:2008.12202](#)].
- [124] S. S. Mishra and V. Sahni, *Primordial Black Holes from a tiny bump/dip in the Inflaton potential*, *JCAP* **04** (2020) 007, [[arXiv:1911.00057](#)].
- [125] G. A. Palma, S. Sypsas, and C. Zenteno, *Seeding primordial black holes in multifield inflation*, *Phys. Rev. Lett.* **125** (2020), no. 12 121301, [[arXiv:2004.06106](#)].
- [126] J. Fumagalli, S. Renaux-Petel, J. W. Ronayne, and L. T. Witkowski, *Turning in the landscape: A new mechanism for generating primordial black holes*, *Phys. Lett. B* **841** (2023) 137921, [[arXiv:2004.08369](#)].
- [127] M. Braglia, D. K. Hazra, F. Finelli, G. F. Smoot, L. Sriramkumar, and A. A. Starobinsky, *Generating PBHs and small-scale GWs in two-field models of inflation*, *JCAP* **08** (2020) 001, [[arXiv:2005.02895](#)].
- [128] S. Pi, Y.-l. Zhang, Q.-G. Huang, and M. Sasaki, *Scalaron from R^2 -gravity as a heavy field*, *JCAP* **05** (2018) 042, [[arXiv:1712.09896](#)].
- [129] X. Wang, Y.-l. Zhang, and M. Sasaki, *Enhanced curvature perturbation and primordial black hole formation in two-stage inflation with a break*, *JCAP* **07** (2024) 076, [[arXiv:2404.02492](#)].
- [130] Z. Zhou, J. Jiang, Y.-F. Cai, M. Sasaki, and S. Pi, *Primordial black holes and gravitational waves from resonant amplification during inflation*, *Phys. Rev. D* **102** (Nov, 2020) 103527.
- [131] Z.-Z. Peng, C. Fu, J. Liu, Z.-K. Guo, and R.-G. Cai, *Gravitational waves from resonant amplification of curvature perturbations during inflation*, *JCAP* **10** (2021) 050, [[arXiv:2106.11816](#)].
- [132] H. V. Ragavendra, L. Sriramkumar, and J. Silk, *Could PBHs and secondary GWs have originated from squeezed initial states?*, *JCAP* **05** (2021) 010, [[arXiv:2011.09938](#)].
- [133] G. Domènech and S. Pi, *NANOGrav hints on planet-mass primordial black holes*, *Sci. China Phys. Mech. Astron.* **65** (2022), no. 3 230411, [[arXiv:2010.03976](#)].
- [134] K. Harigaya, K. Inomata, and T. Terada, *Induced gravitational waves with kination era for recent pulsar timing array signals*, *Phys. Rev. D* **108** (2023), no. 12 123538, [[arXiv:2309.00228](#)].
- [135] Z.-C. Zhao, Q.-H. Zhu, S. Wang, and X. Zhang, *Exploring the Equation of State of the Early Universe: Insights from BBN, CMB, and PTA Observations*, [arXiv:2307.13574](#).
- [136] S. Choudhury, K. Dey, and A. Karde, *Untangling PBH overproduction in w -SIGWs generated by Pulsar Timing Arrays for MST-EFT of single field inflation*, [arXiv:2311.15065](#).
- [137] G. Domènech, S. Pi, A. Wang, and J. Wang, *Induced Gravitational Wave interpretation of PTA*

data: a complete study for general equation of state, [arXiv:2402.18965](#).

- [138] S. Bhattacharya, *Primordial Black Hole Formation in Non-Standard Post-Inflationary Epochs, Galaxies* **11** (2023), no. 1 35, [[arXiv:2302.12690](#)].
- [139] G. Domènech, *Induced gravitational waves in a general cosmological background, Int. J. Mod. Phys. D* **29** (2020), no. 03 2050028, [[arXiv:1912.05583](#)].
- [140] G. Domènech, S. Pi, and M. Sasaki, *Induced gravitational waves as a probe of thermal history of the universe, JCAP* **08** (2020) 017, [[arXiv:2005.12314](#)].
- [141] C. T. Byrnes, P. S. Cole, and S. P. Patil, *Steepest growth of the power spectrum and primordial black holes, JCAP* **06** (2019) 028, [[arXiv:1811.11158](#)].
- [142] A. D. Dolgov and A. D. Linde, *Baryon Asymmetry in Inflationary Universe, Phys. Lett. B* **116** (1982) 329.
- [143] L. Kofman, A. D. Linde, and A. A. Starobinsky, *Towards the theory of reheating after inflation, Phys. Rev. D* **56** (1997) 3258–3295, [[hep-ph/9704452](#)].
- [144] M. A. Amin, M. P. Hertzberg, D. I. Kaiser, and J. Karouby, *Nonperturbative Dynamics Of Reheating After Inflation: A Review, Int. J. Mod. Phys. D* **24** (2014) 1530003, [[arXiv:1410.3808](#)].
- [145] K. D. Lozanov and M. A. Amin, *Self-resonance after inflation: oscillons, transients and radiation domination, Phys. Rev. D* **97** (2018), no. 2 023533, [[arXiv:1710.06851](#)].
- [146] M. A. G. Garcia, K. Kaneta, Y. Mambrini, K. A. Olive, and S. Verner, *Freeze-in from preheating, JCAP* **03** (2022), no. 03 016, [[arXiv:2109.13280](#)].
- [147] M. R. Haque, D. Maity, and P. Saha, *Two-phase reheating: CMB constraints on inflation and dark matter phenomenology, Phys. Rev. D* **102** (2020), no. 8 083534, [[arXiv:2009.02794](#)].
- [148] M. A. G. Garcia, K. Kaneta, Y. Mambrini, and K. A. Olive, *Inflaton Oscillations and Post-Inflationary Reheating, JCAP* **04** (2021) 012, [[arXiv:2012.10756](#)].
- [149] S. Clery, Y. Mambrini, K. A. Olive, and S. Verner, *Gravitational portals in the early Universe, Phys. Rev. D* **105** (2022), no. 7 075005, [[arXiv:2112.15214](#)].
- [150] M. R. Haque and D. Maity, *Gravitational reheating, Phys. Rev. D* **107** (2023), no. 4 043531, [[arXiv:2201.02348](#)].
- [151] M. R. Haque, D. Maity, and R. Mondal, *WIMPs, FIMPs, and Inflaton phenomenology via reheating, CMB and ΔN_{eff} , JHEP* **09** (2023) 012, [[arXiv:2301.01641](#)].
- [152] M. Kawasaki, K. Kohri, and N. Sugiyama, *MeV scale reheating temperature and thermalization of neutrino background, Phys. Rev. D* **62** (2000) 023506, [[astro-ph/0002127](#)].
- [153] S. Hannestad, *What is the lowest possible reheating temperature?, Phys. Rev. D* **70** (2004) 043506, [[astro-ph/0403291](#)].
- [154] M. S. Turner, *Coherent scalar-field oscillations in an expanding universe, Phys. Rev. D* **28** (Sep, 1983) 1243–1247.
- [155] R. Durrer, *The Cosmic Microwave Background*. Cambridge University Press, Cambridge, 2008.
- [156] W. H. Press and P. Schechter, *Formation of galaxies and clusters of galaxies by selfsimilar gravitational condensation, Astrophys. J.* **187** (1974) 425–438.
- [157] J. M. Bardeen, J. R. Bond, N. Kaiser, and A. S. Szalay, *The Statistics of Peaks of Gaussian Random Fields, Astrophys. J.* **304** (1986) 15–61.
- [158] I. Musco, *The threshold for primordial black holes: dependence on the shape of the cosmological perturbations, arXiv:1809.02127*.
- [159] C.-M. Yoo, T. Harada, J. Garriga, and K. Kohri, *Primordial black hole abundance from random*

- Gaussian curvature perturbations and a local density threshold*, *PTEP* **2018** (2018), no. 12 123E01, [[arXiv:1805.03946](#)].
- [160] S. Young, *The primordial black hole formation criterion re-examined: parameterisation, timing, and the choice of window function*, [arXiv:1905.01230](#).
- [161] A. Escrivà, C. Germani, and R. K. Sheth, *Universal threshold for primordial black hole formation*, *Phys. Rev. D* **101** (2020), no. 4 044022, [[arXiv:1907.13311](#)].
- [162] I. Musco, V. De Luca, G. Franciolini, and A. Riotto, *Threshold for primordial black holes. II. A simple analytic prescription*, *Phys. Rev. D* **103** (2021), no. 6 063538, [[arXiv:2011.03014](#)].
- [163] A. D. Gow, C. T. Byrnes, P. S. Cole, and S. Young, *The power spectrum on small scales: Robust constraints and comparing PBH methodologies*, *JCAP* **02** (2021) 002, [[arXiv:2008.03289](#)].
- [164] T. Harada, C.-M. Yoo, and Y. Koga, *Revisiting compaction functions for primordial black hole formation*, *Phys. Rev. D* **108** (2023), no. 4 043515, [[arXiv:2304.13284](#)].
- [165] I. Musco, K. Jedamzik, and S. Young, *Primordial black hole formation during the QCD phase transition: Threshold, mass distribution, and abundance*, *Phys. Rev. D* **109** (2024), no. 8 083506, [[arXiv:2303.07980](#)].
- [166] C. Germani and R. K. Sheth, *The Statistics of Primordial Black Holes in a Radiation-Dominated Universe: Recent and New Results*, *Universe* **9** (2023), no. 9 421, [[arXiv:2308.02971](#)].
- [167] T. Harada, H. Iizuka, Y. Koga, and C.-M. Yoo, *Geometrical origin for the compaction function for primordial black hole formation*, [arXiv:2409.05544](#).
- [168] D. Wands, K. A. Malik, D. H. Lyth, and A. R. Liddle, *A New approach to the evolution of cosmological perturbations on large scales*, *Phys. Rev. D* **62** (2000) 043527, [[astro-ph/0003278](#)].
- [169] B. J. Carr and S. W. Hawking, *Black holes in the early Universe*, *Mon. Not. Roy. Astron. Soc.* **168** (1974) 399–415.
- [170] I. Musco and J. C. Miller, *Primordial black hole formation in the early universe: critical behaviour and self-similarity*, *Class. Quant. Grav.* **30** (2013) 145009, [[arXiv:1201.2379](#)].
- [171] I. Musco, J. C. Miller, and A. G. Polnarev, *Primordial black hole formation in the radiative era: Investigation of the critical nature of the collapse*, *Class. Quant. Grav.* **26** (2009) 235001, [[arXiv:0811.1452](#)].
- [172] I. Hawke and J. M. Stewart, *The dynamics of primordial black hole formation*, *Class. Quant. Grav.* **19** (2002) 3687–3707.
- [173] J. C. Niemeyer and K. Jedamzik, *Near-critical gravitational collapse and the initial mass function of primordial black holes*, *Phys. Rev. Lett.* **80** (1998) 5481–5484, [[astro-ph/9709072](#)].
- [174] A. Escrivà and A. E. Romano, *Effects of the shape of curvature peaks on the size of primordial black holes*, *JCAP* **05** (2021) 066, [[arXiv:2103.03867](#)].
- [175] A. Escrivà, *Simulation of primordial black hole formation using pseudo-spectral methods*, *Phys. Dark Univ.* **27** (2020) 100466, [[arXiv:1907.13065](#)].
- [176] A. Escrivà, C. Germani, and R. K. Sheth, *Analytical thresholds for black hole formation in general cosmological backgrounds*, *JCAP* **01** (2021) 030, [[arXiv:2007.05564](#)].
- [177] A. Escrivà, *PBH Formation from Spherically Symmetric Hydrodynamical Perturbations: A Review*, *Universe* **8** (2022), no. 2 66, [[arXiv:2111.12693](#)].
- [178] C. R. Evans and J. S. Coleman, *Observation of critical phenomena and selfsimilarity in the gravitational collapse of radiation fluid*, *Phys. Rev. Lett.* **72** (1994) 1782–1785, [[gr-qc/9402041](#)].
- [179] D. Maison, *Nonuniversality of critical behavior in spherically symmetric gravitational collapse*, *Phys. Lett. B* **366** (1996) 82–84, [[gr-qc/9504008](#)].

- [180] A. Escrivà, F. Kuhnel, and Y. Tada, *Primordial Black Holes*, [arXiv:2211.05767](#).
- [181] C. Germani and I. Musco, *Abundance of Primordial Black Holes Depends on the Shape of the Inflationary Power Spectrum*, *Phys. Rev. Lett.* **122** (2019), no. 14 141302, [[arXiv:1805.04087](#)].
- [182] S. Young, I. Musco, and C. T. Byrnes, *Primordial black hole formation and abundance: contribution from the non-linear relation between the density and curvature perturbation*, *JCAP* **1911** (2019), no. 11 012, [[arXiv:1904.00984](#)].
- [183] V. De Luca, G. Franciolini, A. Kehagias, M. Peloso, A. Riotto, and C. Unal, *The Ineludible non-Gaussianity of the Primordial Black Hole Abundance*, *JCAP* **1907** (2019) 048, [[arXiv:1904.00970](#)].
- [184] D. K. Hazra, L. Sriramkumar, and J. Martin, *BINGO: A code for the efficient computation of the scalar bi-spectrum*, *JCAP* **05** (2013) 026, [[arXiv:1201.0926](#)].
- [185] D. G. Figueroa, S. Raatikainen, S. Rasanen, and E. Tomberg, *Non-Gaussian Tail of the Curvature Perturbation in Stochastic Ultraslow-Roll Inflation: Implications for Primordial Black Hole Production*, *Phys. Rev. Lett.* **127** (2021), no. 10 101302, [[arXiv:2012.06551](#)].
- [186] Y.-F. Cai, X.-H. Ma, M. Sasaki, D.-G. Wang, and Z. Zhou, *Highly non-Gaussian tails and primordial black holes from single-field inflation*, *JCAP* **12** (2022) 034, [[arXiv:2207.11910](#)].
- [187] T. Harada, C.-M. Yoo, and K. Kohri, *Threshold of primordial black hole formation*, *Phys. Rev. D* **88** (2013), no. 8 084051, [[arXiv:1309.4201](#)]. [Erratum: *Phys.Rev.D* 89, 029903 (2014)].
- [188] H. V. Ragavendra and L. Sriramkumar, *Observational Imprints of Enhanced Scalar Power on Small Scales in Ultra Slow Roll Inflation and Associated Non-Gaussianities*, *Galaxies* **11** (2023), no. 1 34, [[arXiv:2301.08887](#)].
- [189] B. J. Carr, K. Kohri, Y. Sendouda, and J. Yokoyama, *New cosmological constraints on primordial black holes*, *Phys. Rev. D* **81** (2010) 104019, [[arXiv:0912.5297](#)].
- [190] A. Arbey, J. Auffinger, and J. Silk, *Constraining primordial black hole masses with the isotropic gamma ray background*, *Phys. Rev. D* **101** (2020), no. 2 023010, [[arXiv:1906.04750](#)].
- [191] V. Poulin, J. Lesgourgues, and P. D. Serpico, *Cosmological constraints on exotic injection of electromagnetic energy*, *JCAP* **03** (2017) 043, [[arXiv:1610.10051](#)].
- [192] S. Clark, B. Dutta, Y. Gao, L. E. Strigari, and S. Watson, *Planck Constraint on Relic Primordial Black Holes*, *Phys. Rev. D* **95** (2017), no. 8 083006, [[arXiv:1612.07738](#)].
- [193] H. Niikura et al., *Microlensing constraints on primordial black holes with Subaru/HSC Andromeda observations*, *Nature Astron.* **3** (2019), no. 6 524–534, [[arXiv:1701.02151](#)].
- [194] D. Croon, D. McKeen, N. Raj, and Z. Wang, *Subaru-HSC through a different lens: Microlensing by extended dark matter structures*, *Phys. Rev. D* **102** (2020), no. 8 083021, [[arXiv:2007.12697](#)].
- [195] K. Griest, A. M. Cieplak, and M. J. Lehner, *Experimental Limits on Primordial Black Hole Dark Matter from the First 2 yr of Kepler Data*, *Astrophys. J.* **786** (2014), no. 2 158, [[arXiv:1307.5798](#)].
- [196] J. R. Espinosa, D. Racco, and A. Riotto, *A Cosmological Signature of the SM Higgs Instability: Gravitational Waves*, *JCAP* **09** (2018) 012, [[arXiv:1804.07732](#)].
- [197] K. Kohri and T. Terada, *Semianalytic calculation of gravitational wave spectrum nonlinearly induced from primordial curvature perturbations*, *Phys. Rev. D* **97** (2018), no. 12 123532, [[arXiv:1804.08577](#)].
- [198] K. N. Ananda, C. Clarkson, and D. Wands, *The Cosmological gravitational wave background from primordial density perturbations*, *Phys. Rev. D* **75** (2007) 123518, [[gr-qc/0612013](#)].
- [199] D. Baumann, P. J. Steinhardt, K. Takahashi, and K. Ichiki, *Gravitational Wave Spectrum*

- Induced by Primordial Scalar Perturbations*, *Phys. Rev. D* **76** (2007) 084019, [[hep-th/0703290](#)].
- [200] R. Saito and J. Yokoyama, *Gravitational wave background as a probe of the primordial black hole abundance*, *Phys. Rev. Lett.* **102** (2009) 161101, [[arXiv:0812.4339](#)]. [Erratum: *Phys.Rev.Lett.* 107, 069901 (2011)].
- [201] R. Saito and J. Yokoyama, *Gravitational-Wave Constraints on the Abundance of Primordial Black Holes*, *Prog. Theor. Phys.* **123** (2010) 867–886, [[arXiv:0912.5317](#)]. [Erratum: *Prog.Theor.Phys.* 126, 351–352 (2011)].
- [202] K. Inomata, K. Kohri, T. Nakama, and T. Terada, *Enhancement of Gravitational Waves Induced by Scalar Perturbations due to a Sudden Transition from an Early Matter Era to the Radiation Era*, *Phys. Rev. D* **100** (2019) 043532, [[arXiv:1904.12879](#)]. [Erratum: *Phys.Rev.D* 108, 049901 (2023)].
- [203] N. Bhaumik and R. K. Jain, *Small scale induced gravitational waves from primordial black holes, a stringent lower mass bound, and the imprints of an early matter to radiation transition*, *Phys. Rev. D* **104** (2021), no. 2 023531, [[arXiv:2009.10424](#)].
- [204] C. J. Moore, R. H. Cole, and C. P. L. Berry, *Gravitational-wave sensitivity curves*, *Class. Quant. Grav.* **32** (2015), no. 1 015014, [[arXiv:1408.0740](#)].
- [205] N. Bartolo et al., *Science with the space-based interferometer LISA. IV: Probing inflation with gravitational waves*, *JCAP* **12** (2016) 026, [[arXiv:1610.06481](#)].
- [206] Seiji Kawamura et al., *The japanese space gravitational wave antenna: Decigo*, *Classical and Quantum Gravity* **28** (apr, 2011) 094011.
- [207] **DECIGO working group** Collaboration, S. Kawamura, *Primordial gravitational wave and DECIGO*, *PoS KMI2019* (2019) 019.
- [208] J. Crowder and N. J. Cornish, *Beyond LISA: Exploring future gravitational wave missions*, *Phys. Rev. D* **72** (2005) 083005, [[gr-qc/0506015](#)].
- [209] V. Corbin and N. J. Cornish, *Detecting the cosmic gravitational wave background with the big bang observer*, *Class. Quant. Grav.* **23** (2006) 2435–2446, [[gr-qc/0512039](#)].
- [210] J. Baker et al., *Space Based Gravitational Wave Astronomy Beyond LISA*, *Bull. Am. Astron. Soc.* **51** (2019), no. 7 243, [[arXiv:1907.11305](#)].
- [211] **MAGIS-100** Collaboration, J. Coleman, *Matter-wave Atomic Gradiometer Interferometric Sensor (MAGIS-100) at Fermilab*, *PoS ICHEP2018* (2019) 021, [[arXiv:1812.00482](#)].
- [212] **LIGO Scientific, Virgo** Collaboration, B. P. Abbott et al., *Upper Limits on the Stochastic Gravitational-Wave Background from Advanced LIGO’s First Observing Run*, *Phys. Rev. Lett.* **118** (2017), no. 12 121101, [[arXiv:1612.02029](#)]. [Erratum: *Phys.Rev.Lett.* 119, 029901 (2017)].
- [213] **LIGO Scientific, Virgo** Collaboration, B. P. Abbott et al., *Search for the isotropic stochastic background using data from Advanced LIGO’s second observing run*, *Phys. Rev. D* **100** (2019), no. 6 061101, [[arXiv:1903.02886](#)].
- [214] B. Sathyaprakash et al., *Scientific Objectives of Einstein Telescope*, *Class. Quant. Grav.* **29** (2012) 124013, [[arXiv:1206.0331](#)]. [Erratum: *Class.Quant.Grav.* 30, 079501 (2013)].
- [215] **LIGO Scientific** Collaboration, B. P. Abbott et al., *Exploring the Sensitivity of Next Generation Gravitational Wave Detectors*, *Class. Quant. Grav.* **34** (2017), no. 4 044001, [[arXiv:1607.08697](#)].
- [216] M. Giovannini, *Thermal history of the plasma and high-frequency gravitons*, *Class. Quant. Grav.* **26** (2009) 045004, [[arXiv:0807.4317](#)].
- [217] S. Pi, M. Sasaki, A. Wang, and J. Wang, *Revisiting the ultraviolet tail of the primordial gravitational wave*, *Phys. Rev. D* **110** (2024), no. 10 103529, [[arXiv:2407.06066](#)].

- [218] T. N. Collaboration, *The nanograv 15-year data set*, Jun, 2023. For a full author list, see: Gabriella Agazie et al 2023 ApJL 951 L9.
- [219] A. Mitridate, D. Wright, R. von Eckardstein, T. Schröder, J. Nay, K. Olum, K. Schmitz, and T. Trickle, *PTArcade*, [arXiv:2306.16377](#).
- [220] H. Niikura, M. Takada, S. Yokoyama, T. Sumi, and S. Masaki, *Constraints on Earth-mass primordial black holes from OGLE 5-year microlensing events*, *Phys. Rev. D* **99** (2019), no. 8 083503, [[arXiv:1901.07120](#)].
- [221] J. A. Ellis, M. Vallisneri, S. R. Taylor, and P. T. Baker, “Enterprise: Enhanced numerical toolbox enabling a robust pulsar inference suite.” Zenodo, Sept., 2020.
- [222] R. W. Hellings and G. S. Downs, *Upper limits on the isotropic gravitational radiation background from pulsar timing analysis.*, *The Astrophysical Journal Letter* **265** (Feb., 1983) L39–L42.
- [223] **NANOGrav** Collaboration, *KDE Representations of the Gravitational Wave Background Free Spectra Present in the NANOGrav 15-Year Dataset*, July, 2023.
- [224] J. C. Mather et al., *Measurement of the Cosmic Microwave Background Spectrum by the COBE FIRAS Instrument*, *The Astrophysical Journal* **420** (Jan., 1994) 439.
- [225] J. Chluba, A. L. Erickcek, and I. Ben-Dayan, *Probing the Inflaton: Small-scale Power Spectrum Constraints from Measurements of the Cosmic Microwave Background Energy Spectrum*, *The astrophysical Journal* **758** (Oct., 2012) 76, [[arXiv:1203.2681](#)].
- [226] D. Jeong, J. Pradler, J. Chluba, and M. Kamionkowski, *Silk Damping at a Redshift of a Billion: New Limit on Small-Scale Adiabatic Perturbations*, *Phys. Rev. Lett.* **113** (Aug., 2014) 061301, [[arXiv:1403.3697](#)].
- [227] A. Kogut et al., *The Primordial Inflation Explorer (PIXIE): a nulling polarimeter for cosmic microwave background observations*, *JCAP* **2011** (July, 2011) 025, [[arXiv:1105.2044](#)].
- [228] J. Chluba et al., *New horizons in cosmology with spectral distortions of the cosmic microwave background*, *Experimental Astronomy* **51** (June, 2021) 1515–1554, [[arXiv:1909.01593](#)].
- [229] M. Giovannini, *Gravitational waves constraints on postinflationary phases stiffer than radiation*, *Phys. Rev. D* **58** (1998) 083504, [[hep-ph/9806329](#)].
- [230] M. Giovannini, *Production and detection of relic gravitons in quintessential inflationary models*, *Phys. Rev. D* **60** (1999) 123511, [[astro-ph/9903004](#)].
- [231] A. Riazuelo and J.-P. Uzan, *Quintessence and gravitational waves*, *Phys. Rev. D* **62** (2000) 083506, [[astro-ph/0004156](#)].
- [232] N. Seto and J. Yokoyama, *Probing the equation of state of the early universe with a space laser interferometer*, *J. Phys. Soc. Jap.* **72** (2003) 3082–3086, [[gr-qc/0305096](#)].
- [233] L. A. Boyle and A. Buonanno, *Relating gravitational wave constraints from primordial nucleosynthesis, pulsar timing, laser interferometers, and the CMB: Implications for the early Universe*, *Phys. Rev. D* **78** (2008) 043531, [[arXiv:0708.2279](#)].
- [234] A. Stewart and R. Brandenberger, *Observational Constraints on Theories with a Blue Spectrum of Tensor Modes*, *JCAP* **08** (2008) 012, [[arXiv:0711.4602](#)].
- [235] B. Li and P. R. Shapiro, *Precision cosmology and the stiff-amplified gravitational-wave background from inflation: NANOGrav, Advanced LIGO-Virgo and the Hubble tension*, *JCAP* **10** (2021) 024, [[arXiv:2107.12229](#)].
- [236] M. Artymowski, O. Czerwinska, Z. Lalak, and M. Lewicki, *Gravitational wave signals and cosmological consequences of gravitational reheating*, *JCAP* **04** (2018) 046, [[arXiv:1711.08473](#)].
- [237] D. Bettoni, G. Domènech, and J. Rubio, *Gravitational waves from global cosmic strings in*

- quintessential inflation*, *JCAP* **02** (2019) 034, [[arXiv:1810.11117](#)].
- [238] D. G. Figueroa and E. H. Tanin, *Ability of LIGO and LISA to probe the equation of state of the early Universe*, *JCAP* **08** (2019) 011, [[arXiv:1905.11960](#)].
- [239] T. Opferkuch, P. Schwaller, and B. A. Stefanek, *Ricci Reheating*, *JCAP* **07** (2019) 016, [[arXiv:1905.06823](#)].
- [240] N. Bernal and F. Hajkarim, *Primordial Gravitational Waves in Nonstandard Cosmologies*, *Phys. Rev. D* **100** (2019), no. 6 063502, [[arXiv:1905.10410](#)].
- [241] N. Bernal, A. Ghoshal, F. Hajkarim, and G. Lambiase, *Primordial Gravitational Wave Signals in Modified Cosmologies*, *JCAP* **11** (2020) 051, [[arXiv:2008.04959](#)].
- [242] S. Vagnozzi, *Implications of the NANOGrav results for inflation*, *Mon. Not. Roy. Astron. Soc.* **502** (2021), no. 1 L11–L15, [[arXiv:2009.13432](#)].
- [243] S. S. Mishra, V. Sahni, and A. A. Starobinsky, *Curing inflationary degeneracies using reheating predictions and relic gravitational waves*, *JCAP* **05** (2021) 075, [[arXiv:2101.00271](#)].
- [244] M. R. Haque, D. Maity, T. Paul, and L. Sriramkumar, *Decoding the phases of early and late time reheating through imprints on primordial gravitational waves*, *Phys. Rev. D* **104** (2021), no. 6 063513, [[arXiv:2105.09242](#)].
- [245] M. Benetti, L. L. Graef, and S. Vagnozzi, *Primordial gravitational waves from NANOGrav: A broken power-law approach*, *Phys. Rev. D* **105** (2022), no. 4 043520, [[arXiv:2111.04758](#)].
- [246] M. Giovannini, *Inflation, space-borne interferometers and the expansion history of the Universe*, *Eur. Phys. J. C* **82** (2022), no. 9 828, [[arXiv:2206.08217](#)].
- [247] R. Jinno, T. Moroi, and K. Nakayama, *Probing dark radiation with inflationary gravitational waves*, *Phys. Rev. D* **86** (2012) 123502, [[arXiv:1208.0184](#)].
- [248] A. Chakraborty, M. R. Haque, D. Maity, and R. Mondal, *Inflaton phenomenology via reheating in light of primordial gravitational waves and the latest BICEP/Keck data*, *Phys. Rev. D* **108** (2023), no. 2 023515, [[arXiv:2304.13637](#)].
- [249] J. S. Bullock and J. R. Primack, *NonGaussian fluctuations and primordial black holes from inflation*, *Phys. Rev. D* **55** (1997) 7423–7439, [[astro-ph/9611106](#)].
- [250] S. Young, D. Regan, and C. T. Byrnes, *Influence of large local and non-local bispectra on primordial black hole abundance*, *JCAP* **02** (2016) 029, [[arXiv:1512.07224](#)].
- [251] C.-M. Yoo, J.-O. Gong, and S. Yokoyama, *Abundance of primordial black holes with local non-Gaussianity in peak theory*, *JCAP* **09** (2019) 033, [[arXiv:1906.06790](#)].
- [252] H. V. Ragavendra, *Accounting for scalar non-Gaussianity in secondary gravitational waves*, *Phys. Rev. D* **105** (2022), no. 6 063533, [[arXiv:2108.04193](#)].